*Computers & Structures* Vol. 27, No. 4, pp. 541–563, 1987
Printed in Great Britain.

0045-7949/87 $3.00 + 0.00


# THEORETICAL BASIS OF THE PANDA COMPUTER PROGRAM FOR PRELIMINARY DESIGN OF STIFFENED PANELS UNDER COMBINED IN-PLANE LOADS

DAVID BUSHNELL
Lockheed Palo Alto Research Laboratory, 3251 Hanover St., Palo Alto, CA 94304, U.S.A.

(*Received* 20 *November* 1986)

**Abstract**—A theory based on minimum potential energy for the bifurcation buckling of elastic or elastic–plastic isotropic or elastic composite, flat or cylindrical, ring- and stringer-stiffened panels subjected to combined in-plane loads is derived. Equations are given for general instability, panel instability and local instability of panels with fully populated $6 \times 6$ thickness-integrated constitutive matrices. Also derived are equations for crippling and rolling of stiffeners. The theory has been implemented in user-friendly, interactive computer programs called PANDA and PANDA2 for the minimum-weight design of panels. These programs have been described in previous papers.

## NOTATION

| | |
|---|---|
| $A$ | stiffener cross-section area |
| $\mathbf{A}$ | $3 \times 3$ integrated constitutive matrix governing extensional (membrane) behavior, eqn (4) |
| $a_0$, $b_0$ | distances between rings, stringers (Fig. 1) |
| $a$, $b$ | axial, circumferential, dimensions of panel |
| $b_i$ | width of $i$th segment of any stiffener (Fig. 4) |
| $C_{ij}$; $i = 1, 6$; $j = 1, 6$ | $6 \times 6$ integrated constitutive matrix governing extensional and bending behavior, eqns (37) and (40) |
| $c$ | slope of buckling nodal lines for panel that is long in the $x$-direction [eqns (51), Fig. 9(a)] |
| $d$ | slope of buckling nodal lines for panel that is long in the $y$-direction [eqns (51), Fig. 9(b)] |
| $e$ | strain or eccentricity, depending on context |
| $\bar{e}$ | effective strain |
| $E$, $E_0$ | Young's modulus |
| $G$, $G_0$ | shear modulus |
| $\bar{G}$ | reduced shear modulus, eqn (41) |
| $g$ | plasticity factor, eqn (30) |
| $I$ | stiffener bending moment of inertia |
| $J$ | stiffener torsional constant (e.g. $\Sigma_{i=1}^{n} b_i t_i^3/3$) |
| $\bar{n}$, $\bar{m}$ | halfwaves in axial, circumferential directions |
| $n$, $m$ | circumferential, axial wave indices, eqn (52) |
| $n_1$, $m_1$, $n_2$, $m_2$ | wave indices, eqn (51) |
| $N$, $M$ | stress, moment resultants |
| $p$ | pressure |
| $R$ | radius of cylindrical panel |
| $s$ | local coordinate shown in Fig. 13 |
| $t$ | thickness |
| $u^*$, $v^*$, $w^*$ | displacement components referred to stiffener coordinates, Figs 11, 12 |
| $u$, $v$, $w$ | displacement components of panel skin in $x$-, $y$-, $z$-directions, respectively (Fig. 3) |
| $x$, $y$, $z$ | shell surface coordinates, Fig. 2; or coordinates shown in Fig. 13, depending on context |
| $\bar{x}_i$, $\bar{y}_i$ | coordinates in the plane of the $i$th stiffener segment (Fig. 4) |
| $\bar{x}$, $\bar{y}$, $\bar{z}$ | coordinates shown in Figs 11, 12 |
| $x_{max}$, $y_{max}$ | defined just after eqn (49) |
| $\beta$ | rotation of flange, Fig. 13 |
| $\gamma$ | stiffener rolling angle, Fig. 12 |
| $\lambda$ | eigenvalue or load factor |
| $\kappa$ | change in curvature or twist |
| $\nu$ | Poisson's ratio |
| $\rho$ | density |
| $\sigma$ | stress |
| $\bar{\sigma}$ | effective stress |
| $\omega$ | stiffener rotation components, Figs 11, 12 |
| $\phi$ | ratio (local buckling load factor)/(general buckling load factor), or angle from material coordinates of a lamina to the axial coordinate (Fig. 2), depending on context |

*Subscripts*

| | |
|---|---|
| eff | "effective" |
| 1, 2, 11, 12, 22 | pertain to strain components and moduli with respect to the material coordinate directions, 1 and 2, shown in Fig. 2 |
| $b$ | pertaining to buckling analysis |
| $b$ | bending energy [eqns (85), (88), (92), (94)] |
| $e$ | eigenvalue parameter |
| $f$ | flange |
| $i$ | stiffener segment number |
| $m$ | membrane energy [eqns (81)–(83), (90), (91), (93)] |
| $pl$ | material proportional limit |
| *PRE*, fixed | prestress not multiplied by eigenvalue |
| $s$ | secant modulus |
| skin | pertaining to part of the panel between stiffeners |
| $T$ | tangent modulus |
| $w$ | web |
| $\bar{x}$ | $\bar{x}$-direction (Figs 11, 12) |
| $x$ | $x$-direction (Fig. 2), or along stiffener axis |
| $y$ | $y$-direction (Fig. 2) |

| | |
|---|---|
| $xy$ | in-plane shear (Fig. 2), or twist |
| $()_{,x}$ | differentiation with respect to $x$, eqns (5) |

*Superscripts*

| | |
|---|---|
| eff | "effective" |
| $b$ | pertaining to buckling analysis |
| $f$ | flange |
| $i$ | stiffener segment number |
| $j$ | stiffener segment number |
| $k$ | layer index |
| 0 | prebuckling condition at design load |
| $r$ | ring |
| $s$ | stringer |
| $w$ | web |

## INTRODUCTION

### *Background*

An overview of the PANDA computer program is given in [1]. A brief review of the literature on buckling and optimization of stiffened panels appears in that paper and therefore will not be repeated here. However, the theory on which PANDA is based has never been published. Since the PANDA program is widely used for preliminary design, and since much of the theory of PANDA has also been incorporated into PANDA2 [2], it seems appropriate to describe more fully the theoretical basis of PANDA. That is the purpose of this paper.

In PANDA buckling loads are calculated by use of simple assumed displacement functions. For example, general instability of panels with balanced laminates and no shear loading is assumed to occur in the familiar $w(x, y) = C \sin(ny)\sin(mx)$ mode. In the presence of in-plane shear and/or unbalanced laminates, both local and general buckling patterns are assumed to have the form

$$w(x, y) = C\{\cos[(n + mc)y - (m + nd)x] - \cos[(n - mc)y + (m - nd)x]\}$$

in which either $c$ or $d$ are zero, depending on the geometry and the stiffness of the entire panel or whatever portion of the panel is under consideration.

The skin is cylindrical with radius $R$ and the stiffeners are composed of assemblages of flat plate segments the lengths of which are large compared to the widths and the widths of which are large compared to the thicknesses. These flat plate segments are oriented either normal or parallel to the plane of the panel skin.

Figures 1 and 2 show typical panel and stiffener geometry, loading, wall construction and coordinates. The overall dimensions of the panel are $(a, b)$ and the spacings of the stiffeners are $(a_0, b_0)$.

### *Material properties*

If the material is orthotropic or anisotropic, buckling is assumed to occur at stress levels for which this material remains elastic. Feasible designs are constrained by maximum stress or strain criteria. In PANDA plasticity with arbitrary strain hardening is permitted if the material is isotropic or if it has

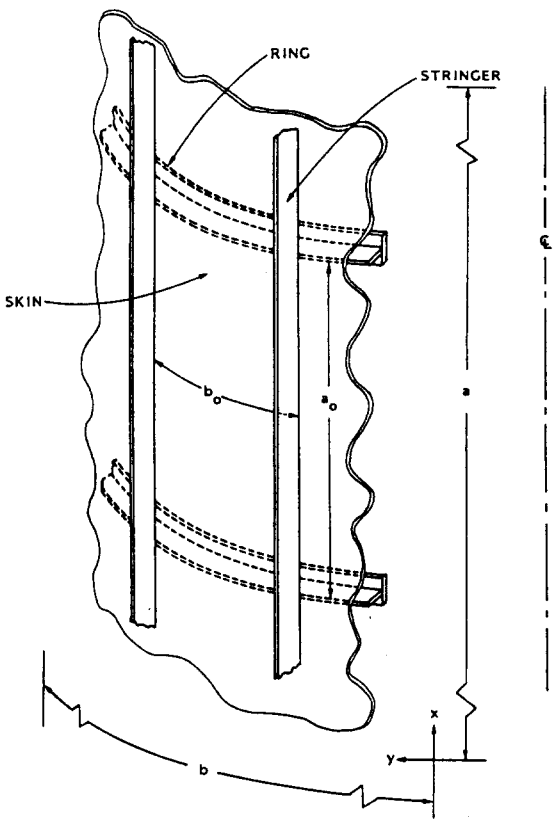


Fig. 1. Stiffened cylindrical panel with overall dimensions $(a, b)$, ring spacing $(a_0)$ and stringer spacing $(b_0)$.

stiffness in one coordinate direction only, as does the continuum representation of each segment of a smeared stiffener. The cylindrical skin and stiffener segments can be composed of multiple layers of isotropic or orthotropic material, as depicted in Fig. 2. Each layer has a unique angle of orthotropy relative in the case of the panel skin to the direction of the generator ($x$-direction) and in the case of a stiffener segment to the stiffener axis. In the buckling analysis the segments of the stiffeners are assumed to be monocoque and isotropic or orthotropic, not layered anisotropic. Therefore, equivalent orthotropic properties for stiffener segments are calculated from input data for the stiffener segment laminates provided by the program user. This limitation does not apply to PANDA2 [2].

### *Types of buckling*

Optimum designs with respect to weight are obtained in the presence of constraints due to local and general buckling, maximum tensile and compressive stress or strain, maximum shear strain, and lower and upper bounds on skin layer thicknesses, stiffener cross-section dimensions and stiffener spacings. Design parameters allowed to vary during the optimization phase include panel skin laminae thickness and winding angles, spacings of stiffeners, and thicknesses and widths of the segments of ring and stringer cross-sections.

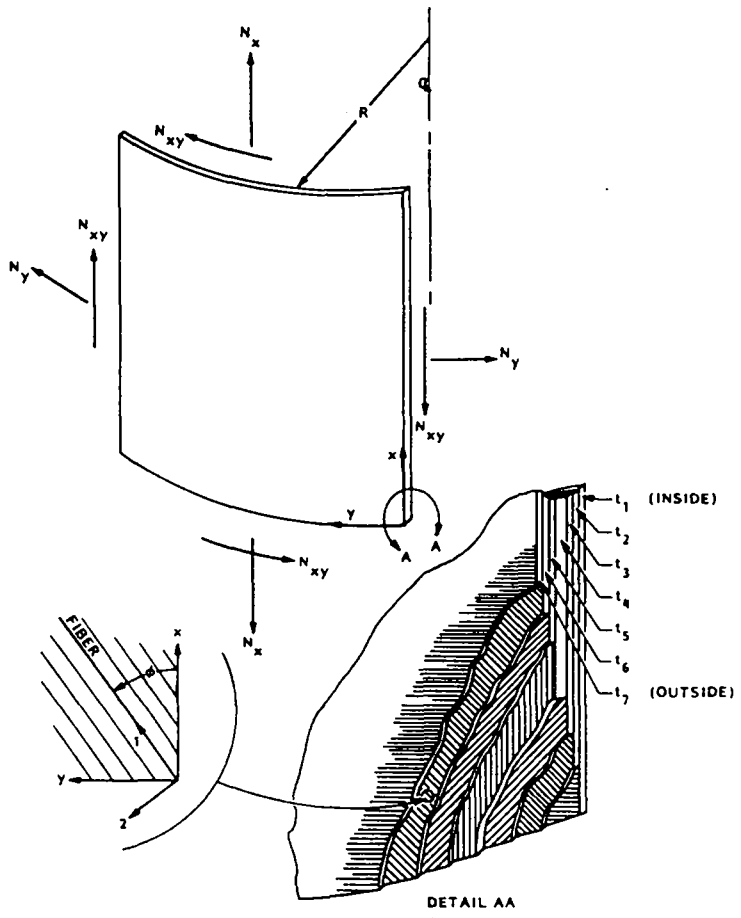


Fig. 2. Coordinates, loading and wall construction.

In PANDA the buckling formulas are derived from Donnell's equations [3] with *a posteriori* application of a reduction factor $(n_c^2 - 1)/n_c^2$ for panels in which the axial half-wavelength of the buckling pattern is longer than the panel radius of curvature, $R$. The circumferential wave index, $n_c$, equals $n\pi R/b$ or $n\pi R/b_0$, with $n$ being the number of half-waves in the circumferential direction over the span $b$ or $b_0$, respectively.

The many types of buckling included in the PANDA analysis are summarized in Table 1 and are briefly described next.

*Skin buckling*

For the case of balanced laminates and no in-plane shear, local buckling of the skin is assumed to have the form

$$w_{skin} = C_{skin} \sin\left(\frac{\bar{n}_{skin}\pi y}{b_0}\right) \sin\left(\frac{\bar{m}_{skin}\pi x}{a_0}\right) \qquad (1)$$

in which $\bar{n}_{skin}$ and $\bar{m}_{skin}$ are the numbers of half-waves between stringers with spacing $b_0$ and rings with spacing $a_0$, respectively. The coordinates and shell wall displacement components are shown in Fig. 3. Equation (1) implies simple-support boundary conditions at stiffener lines of attachment. With shear present and/or unbalanced laminates the skin buckling pattern has the form given in the second paragraph under Background.

*General instability*

General instability buckling modes of panels with balanced laminates and no shear also have the form given in eqn (1), with $a_0$, $b_0$, $\bar{n}_{skin}$ and $\bar{m}_{skin}$ replaced by quantities appropriate to the overall dimensions (a, b) of the panel. PANDA also calculates values for "semi-general" instability, that is, buckling between rings with smeared stringers and buckling between stringers with smeared rings.

*Buckling of stiffeners*

Local buckling of the $i$th stiffener segment implies

$$w^i_{stiff} = C^i_{stiff} \sin\left(\frac{\pi \bar{y}_i}{b_i}\right) \sin\left(\frac{\bar{m}^i_{stiff}\pi \bar{x}}{l}\right) \qquad (2)$$

for each stiffener segment with both long edges supported (called "internal" segments in Fig. 4). As shown in Fig. 4 the quantity $\bar{x}$ is the coordinate along the stiffener axis, $\bar{y}_i$ is the coordinate perpendicular to $\bar{x}$ in the plane of the $i$th stiffener segment, $b_i$ is the

Table 1. Buckling modes included in the PANDA analysis

| Type of buckling | Model used for estimate |
|---|---|
| 1. General instability [Fig. 1; eqn (57)] | Buckling of skin and stiffeners together with smeared rings and stringers. Panel is simply supported along the edges $x = y = 0$, $x = a$ and $y = b$ |
| 2. Local instability [Fig. 3; eqn (57)] | Buckling of skin between adjacent rings and adjacent stringers. Portion of panel bounded by adjacent stiffeners is simply supported. Stiffeners take their share of the load in the prebuckling analysis but are disregarded in the stability analysis |
| 3. Panel instability (a) between rings with smeared stringers [Fig. 1; eqn (57)] | Buckling of skin and stringers between adjacent rings. Portion of panel bounded by adjacent rings is simply supported. Stringers are smeared. Simple support conditions imposed at $y = 0$ and at $y = b$. Rings take their share of the load in the prebuckling analysis, but are disregarded in the stability analysis |
| (b) between stringers with smeared rings [Fig. 1; eqn (57)] | Buckling of skin and rings between adjacent stringers. Portion of panel between adjacent stringers is simply supported. Rings are smeared. Simple support conditions imposed at $x = 0$ and at $x = a$. Stringers take their share of the load in the prebuckling analysis, but are disregarded in the stability analysis |
| 4. Local crippling of stiffener segments (a) "internal" segments [Figs 4,5; eqn (71)] | Individual stiffener segment buckles as if it were a long flat strip simply supported along its two long edges. Loading is compression along the stiffener axis. Curvature of ring segments ignored |
| (b) "end" segments [Figs 4,5; eqn (79)] | Individual stiffener segment buckles as if it were a long flat strip simply supported along the long edge at which it is attached to its neighboring segment or to the panel skin and free along the opposite edge. Loading is compression along the stiffener axis. Number of half waves along the stiffener axis is the same as that of the part of the structure to which the "end" is attached. Curvature of ring segments ignored |
| 5. Local rolling with skin buckling between stiffeners [Fig. 6(a); eqns (57), (96), (97)] | Same as "local instability" except that strain energy in stiffeners and work done by prebuckling compression in stiffeners are included in the buckling formula. Stiffener cross-sections do not deform as stiffeners twist about their lines of attachment to the panel skin |
| 6. Rolling instability (a) with smeared stringers [Fig. 6(a); eqns (57), (96), (97)] | Same as "panel instability", type (a), except that strain energy of rings and work done by prebuckling compression along the ring centroidal axis are included in the buckling formula. Ring cross-section does not deform as ring twists about its line of attachment to the panel skin |
| (b) with smeared rings [Fig. 6(a); eqns (57), (96), (97)] | Same as "panel instability", type (b), except that strain energy of stringers and work done by prebuckling compression along the stringer centroidal axis are included in the buckling formula. Stringer cross-section does not deform as it twists about its line of attachment to the panel skin |
| 7. Rolling of stringers, no buckling of skin [Fig. 6(b); eqns (112), (119)] | Stringer web cross-section deforms but the flange cross-section does not. Buckling mode has waves along stiffener axis |
| 8. Rolling of rings, no buckling of skin [Fig. 6(b); eqns (112), (119)] | Ring web cross-section deforms but the flange cross-section does not. Buckling mode has waves along the ring axis. This mode is sometimes called "frame tripping" by those interested in submarine structures |
| 9. Axisymmetric rolling of rings, no skin buckling [Fig. 6(c); eqns (112), (119)] | Same as "rolling of rings", except that the buckling mode has zero waves around the circumference of the panel |

width of the stiffener segment, and $l$ is the length of the stiffener segment. ($l = a_0$ for stringers and $l = b_0$ for rings.) For stiffener segments with only one long edge supported (called "end" segments), the local buckling modal displacement is assumed to be in the form

$$w^i_{\text{stiff}} = C^i_{\text{stiff}} \bar{y}_i \sin\left(\frac{\bar{m}^i_{\text{stiff}} \pi \bar{x}}{l}\right). \tag{3}$$

The stiffener segment buckling analysis is carried out with the assumption that each "internal" segment buckles with its own $\bar{m}^i$. This assumption implies that rotational incompatibility exists at junctions between segments with differing critical values of $\bar{m}^i$. "End" segments are assumed to buckle at the critical $\bar{m}^i$ of the segment to which they are joined. The buckling modes (2) and (3) are shown in Fig. 5.

*Rolling modes*

Additional types of panel and stiffener buckling are considered by PANDA. These are called "rolling" modes. The first kind of rolling mode involves both skin and stiffeners and is local or "semi-general", the characteristic half-wavelength being integer fractions of the lengths $(a_0, b_0)$, or $(a, b_0)$ or $(a_0, b)$. In these rolling modes the stiffener cross-sections rotate about their lines of attachment to the panel skin as shown in Fig. 6(a). The cross-sections do not deform in the plane of the paper. They do warp, however. The other types of rolling instability do not involve the

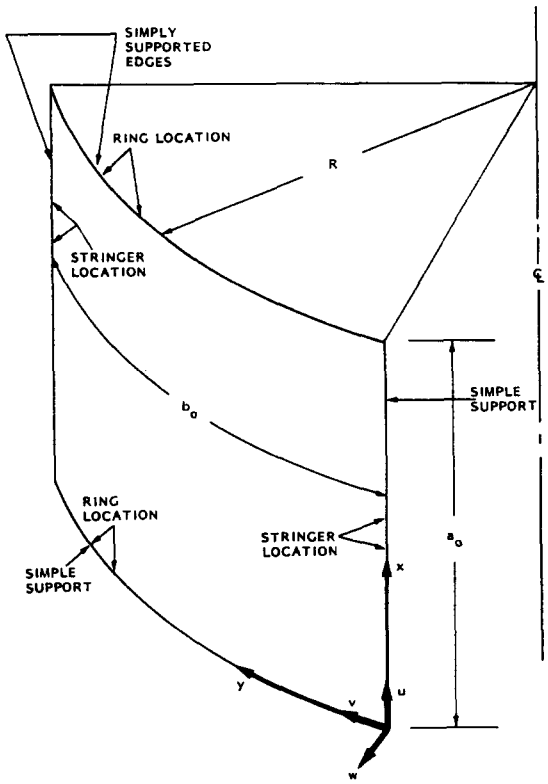


Fig. 3. Cylindrical panel between stiffeners: displacement components $u$, $v$, $w$, and coordinates for local skin buckling.

skin at all. Only the stiffener web deforms, the rest of the stiffener cross-section displacing and rotating as a rigid body, as displayed in Fig. 6(b). One of these rolling modes [Fig. 6(b)] occurs in both rings and stringers and in both curved and flat panels. In this mode the buckling deformations are nonuniform (sinusoidal) along with axis of the stiffener. The other rolling mode [Fig. 6(c)] occurs only in the cases of internal rings on cylindrical panels under external pressure and external rings on cylindrical panels under internal pressure. In this mode buckling deformations are uniform along the axis of the ring. Stiffener rolling in the more general mode [Fig. 6(b)] is due to compression along the stiffener and is only weakly dependent on the curvature of this axis. On the other hand, the local ring buckling depicted in Fig. 6(c) is axisymmetric and arises because of the circumferential curvature of the stiffener axis and prestress in the stiffener segments. It is interesting to note that axisymmetric rolling can occur even if there are no compressive stresses anywhere in the structure, as is the case for internally pressurized cylindrical shells with external rings.

## PREBUCKLING AND BUCKLING ANALYSIS ON WHICH PANDA IS BASED

### *Prebuckling analysis*

The prebuckling analysis is based on the assumption that the panel with smeared stiffeners is in a

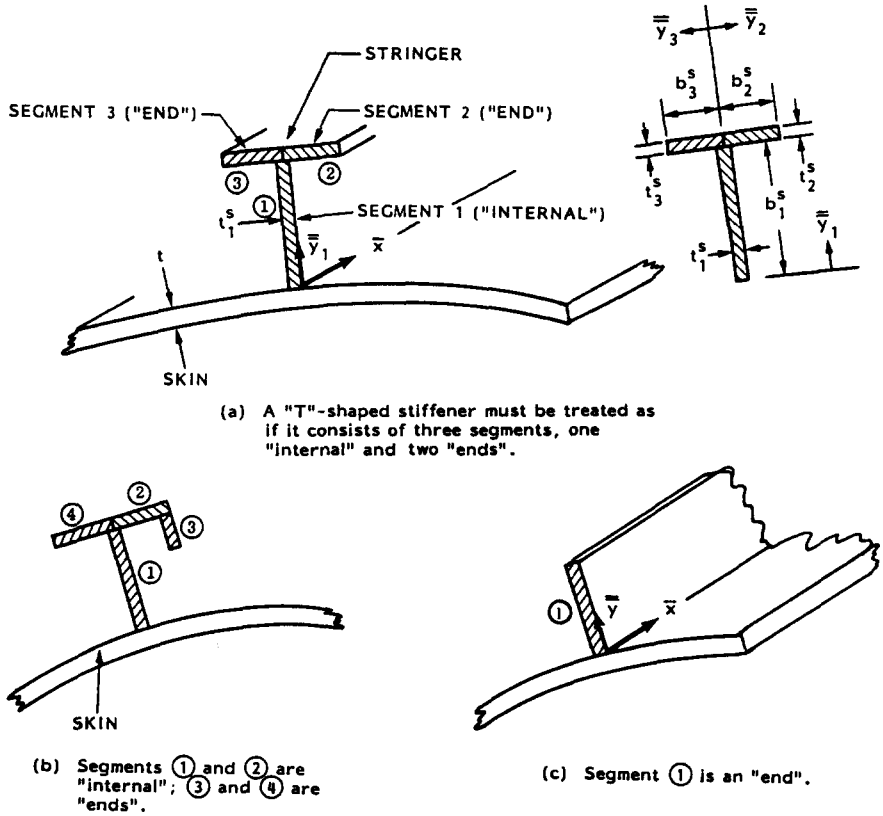


Fig. 4. Stiffener nomenclature and local coordinates $\bar{x}$ and $\bar{y}_i$.

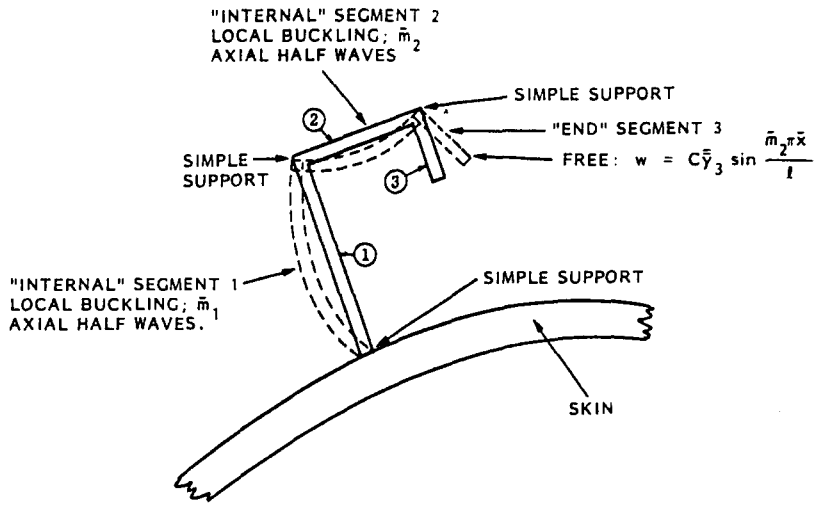


EACH "INTERNAL" STIFFENER SEGMENT IS ASSUMED TO BE SIMPLY-SUPPORTED AT ITS EDGES. THE "END" SEGMENT REMAINS STRAIGHT IN THE WIDTH COORDINATE AS SEGMENTS 2 AND 3 BUCKLE TOGETHER WITH THE SAME $\bar{m} = \bar{m}_2$.

Fig. 5. Local buckling of stiffener segments.

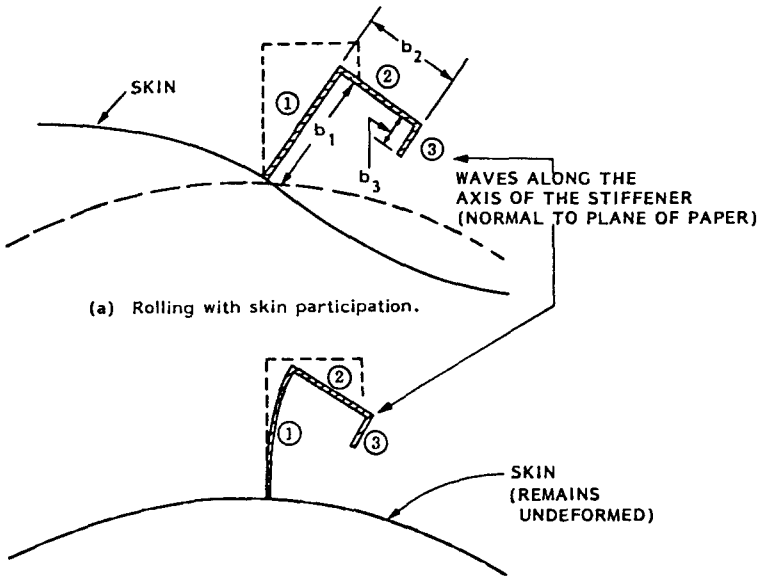


(a) Rolling with skin participation.

(b) No skin participation, wavy buckles.

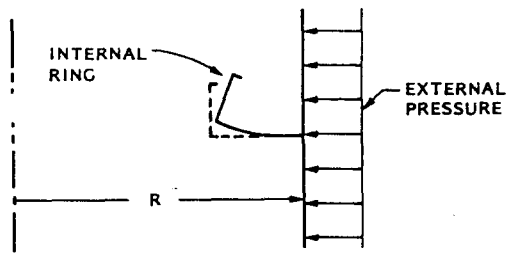


(c) No skin participation; axisymmetric sidesway.

Fig. 6. Three types of "rolling" of a stiffener.

membrane state of strain $\mathbf{e}^0$. The membrane strain components can be determined from:

$$\mathbf{e}^0 \equiv \begin{Bmatrix} e_x^0 \\ e_y^0 \\ e_{xy}^0 \end{Bmatrix} = [A]^{-1}_{3\times 3} \begin{Bmatrix} N_x^0 \\ N_y^0 \\ N_{xy}^0 \end{Bmatrix} \tag{4}$$

in which $N_x^0$, $N_y^0$, $N_{xy}^0$ represent the load combination for which the panel is being designed and A is the $3 \times 3$ integrated constitutive matrix for extensional deformation of the panel with smeared stiffeners. If the materials of the skin and stiffeners remain elastic at the load level specified by the designer then the entire prebuckling analysis consists of: (1) an approximate determination of the circumferential strain midway between rings and circumferential strain at ring centroids for panels stiffened by rings only, and (2) a computation from the known strain field and known material properties of how much of the total load $N_x^0$, $N_y^0$ is carried by the skin and how much is carried by the stiffeners. (The in-plane shear load $N_{xy}^0$ is carried only by the skin.)

*Calculation of midbay circumferential strain.* In the case of panels or complete cylindrical shells stiffened by rings and subjected to uniform laterial pressure, the stress in the skin midway between rings can be rather sensitive to the ring cross-section areas and spacing for configurations with rather closely spaced rings. Such configurations represent optimum designs of submarine pressure hulls, for example. The buckling pressure corresponding to local instability depends directly on the midbay circumferential stess. When the material behavior is nonlinear, the buckling pressure corresponding to general instability also depends on the state of strain at midbay because the reduced moduli of the skin there naturally act to decrease the coefficients $C_{ij}$ of the integrated constitutive law which appear in the buckling equations.

The differential equation governing the axisymmetric prebuckling behavior of a composite cylindrical shell supported in any way at its ends is derived by Jones and Hennemann [4]:

$$Aw^0_{,xxxx} + Bw^0_{,xx} + Dw^0 + E = 0 \tag{5}$$

with the coefficients $A$, $B$, $D$, and $E$ given by:

$$\begin{aligned} A &= C_{44} - C_{14}^2/C_{11} \\ B &= -N_x^0 + 2(C_{12}C_{14} - C_{11}C_{15})/(C_{11}R) \\ D &= (C_{22} - C_{12}^2/C_{11})/R^2 \\ E &= C_{12}N_x^0/(C_{11}R) - N_y^0/R \end{aligned} \tag{6}$$

in which the $C_{ij}$ are coefficients of the integrated constitutive law relating reference surface strains and changes in curvature of the panel skin to stress and moment resultants in the panel skin (no smeared stiffeners). The homogeneous form of eqn (5) can be written as:

$$w^0_{,xxxx} + 4Sw^0_{,xx} + 4T^2w^0 = 0 \tag{7}$$

where

$$S = B/(4A) \quad T = (D/A)^{1/2}/2. \tag{8}$$

In eqns (5) and (7), the axial coordinate $x$ is zero at the mid-length of the cylinder (midbay). The particular solution of eqn (5) is:

$$w_p^0 = -(C_{12}N_x^0 - C_{11}N_y^0)R/(C_{11}C_{22} - C_{12}^2). \tag{9}$$

Almroth [5] gives the following expression for the axisymmetric normal displacement of a clamped or a simply-supported uniformly loaded cylindrical shell:

$$w^0 = w_p^0[1 + F_1\sin(a_1x)\sinh(a_2x) + F_2\cos(a_1x)\cosh(a_2x)] \tag{10}$$

in which:

$$a_1 = (T + S)^{1/2} \quad a_2 = (T - S)^{1/2}. \tag{11}$$

Equation (10) can be applied to the case of a ring stiffened panel. For this configuration eqn (10) applies to the portion of the panel between adjacent rings. The axial coordinate $x$ is zero midway between rings and equal to $\pm a_0/2$ at the rings. Expression (10) satisfies the symmetry condition at $x = 0$. The unknown coefficients $F_1$ and $F_2$ can be obtained from the two conditions:

$$\frac{dw^0}{dx} = 0 \quad \text{at} \quad x = a_0/2 \tag{12}$$

$$\frac{2}{a_0}\int_0^{(a_0/2)} w^0\,dx = e_y^0R \tag{13}$$

where $e_y^0$ is the average circumferential strain [eqn (4)] calculated from the model in which the stiffeners have been smeared out. The first condition is a symmetry condition and the second condition states that the average radial displacement is equal to that calculated from the smeared ring model [eqn (4)]. Conditions (12) and (13) lead to:

$$\begin{aligned} F_1 &= -B_{22}(a_1^2 + a_2^2)L/\Delta \\ F_2 &= B_{21}(a_1^2 + a_2^2)L/\Delta \end{aligned} \tag{14}$$

with:

$$L \equiv a_0/2$$

$$\Delta \equiv B_{11}B_{22} - B_{12}B_{21}$$

$$B_{11} = a_2\sin(a_1L)\cosh(a_2L) - a_1\cos(a_1L)\sinh(a_2L)$$

$$B_{12} = a_2\cos(a_1L)\sinh(a_2L) + a_1\sin(a_1L)\cosh(a_2L)$$

$$B_{21} = a_2 \sin(a_1 L)\cosh(a_2 L) + a_1 \cos(a_1 L)\sinh(a_2 L)$$

$$B_{22} = a_2 \cos(a_1 L)\sinh(a_2 L) - a_1 \sin(a_1 L)\cosh(a_2 L); \quad (15)$$

the prebuckling radial displacements at $x = 0$ (midway between rings) and at the ring attachment stations are:

$$w^0(x = 0) = w_p^0 + F_2(w_p^0 - e_y^0 R) \quad (16)$$

$$w^0(x = L = a_0/2) = w_p^0 + (w_p^0 - e_y^0 R) \times [F_1 \sin(a_1 L)\sinh(a_2 L) + F_2 \cos(a_1 L)\cosh(a_2 L)]. \quad (17)$$

In certain cases it is important to include the effect of prebuckling axial bending midway between rings. This bending contributes to further plastic straining at the outer fiber of a ring-stiffened, externally pressurized cylindrical shell, leading to a reduction in the instantaneous stiffness coefficients governing stability. The change in axial curvature $w^0_{xx}$ at $x = 0$ is given by:

$$w^0_{xx}(x = 0) = (w_p^0 - e_y^0 R) \times [F_1 2\, a_1 a_2 + F_2(a_2^2 - a_1^2)]. \quad (18)$$

The circumferential strains midway between rings and at ring attachment stations are:

$$e^0_{y\text{skin}}(x = 0) = w^0(x = 0)/R \quad (19a)$$

$$e^0_{y\text{skin}}(x = a_0/2) = w^0(x = a_0/2)/R. \quad (19b)$$

*Loads in the skin and in the stiffeners.* The stress resultants along the axis $\bar{x}$ of each stiffener segment are calculated from the axial strains in these segments, which are available from eqns (4) and (19b). Knowing the strains along the axis of each set of stiffeners and the stress–strain curves of the materials from which these segments are fabricated, one can calculate the stress resultants $N^{0i}_{\bar{x}}$ from:

$$N^{0i}_{\bar{x}} = \sigma^{0i}_{\bar{x}} t^i = E^i_s e^{0i}_{\bar{x}} t^i \quad (20)$$

in which $E^i_s$ is the secant modulus, $e^i_{\bar{x}}$ is the strain of the stiffener axis, and $t^i$ is the thickness of the $i$th stiffener segment.

If local bending of the skin between rings is ignored, the resultants $(N^0_{x\text{skin}}, N^0_{y\text{skin}})$ of the skin are given by:

$$N^0_{x\text{skin}} = N^0_x - \sum_{i=1}^{N^r} N^{0i}_{\bar{x}}(\text{stringer})/b_0 \quad (21)$$

$$N^0_{y\text{skin}} = N^0_y - \sum_{i=1}^{N^r} N^{0i}_{\bar{x}}(\text{ring})/a_0 \quad (22)$$

where $N^s$ and $N^r$ are the numbers of stringer segments and ring segments, respectively. If local bending of the skin between rings is accounted for, the circumferential resultant carried by the skin midway between rings is given by:

$$N^0_{y\text{skin}} = C_{12} N^0_{x\text{skin}}/C_{11} + e^0_{y\text{skin}}(x = 0)[C_{22} - C_{12}^2/C_{11}] \quad (23)$$

with $e^0_{y\text{skin}}$ being computed from eqn (19a).

*Inclusion of plasticity.* The flow of calculations in the prebuckling phase is displayed in Fig. 7. As can be seen from this flow, the process is iterative. The objectives of the prebuckling computations are: (1) to compute instantaneous values for the moduli $E^k_{11}$, $E^k_{12}$, $E^k_{22}$, and $G^k$, $k = 1, 2, \ldots N^L$, where $N^L$ is the number of layers in the panel skin (these moduli are used in the calculation of the integrated constitutive law governing stability); (2) to compute instantaneous values for the corresponding moduli of the segments of the rings and stringers; (3) to compute how much load is carried by the skin and how much is carried by the stiffeners. These goals are summarized in the two boxes in the lower left-hand corner of Fig. 7.

The contents of the boxes on the right-hand-side of Fig. 7 will next be described.

The strain components in the $k$th lamina in material coordinates are calculated from:

$$\begin{Bmatrix} e^k_1 \\ e^k_2 \\ e^k_{12} \end{Bmatrix} = \begin{bmatrix} C^2 & s^2 & sc \\ s^2 & c^2 & -sc \\ -2sc & 2sc & (c^2 - s^2) \end{bmatrix} \begin{Bmatrix} e^0_x - z w^0_{xx} \\ e^0_{y\text{skin}} \\ e^0_{xy} \end{Bmatrix} \quad (24)$$

in which:

$$c \equiv \cos\phi \quad s \equiv \sin\phi \ (\phi \text{ is shown in Fig. 2}), \quad (25)$$

$z$ is the positive outward coordinate normal to the shell reference surface, $w^0_{xx}$ is given by eqn (18), and $e^0_{y\text{skin}}$ is given by eqn (19a). The corresponding stress components are:

$$\sigma^k_1 = E^k_{11} e^k_1 + E^k_{12} e^k_2$$
$$\sigma^k_2 = E^k_{12} e^k_1 + E^k_{22} e^k_2$$
$$\sigma^k_{12} = G^k e^k_{12}. \quad (26)$$

The moduli $E^k_{11}$, $E^k_{12}$, $E^k_{22}$ and $G^k$ may be reduced from the elastic values because of plastic flow. $J_2$-deformation theory [6] is used as described next. Hutchinson [6] gives further details.

The effective stress can be calculated from the stress components $\sigma^k_1$, $\sigma^k_2$, $\sigma^k_{12}$:

$$\bar{\sigma}^k = [(\sigma^k_1)^2 + (\sigma^k_2)^2 - (\sigma^k_1 \sigma^k_2) + 3(\sigma^k_{12})^2]^{1/2}. \quad (27)$$

If $\bar{\sigma}^k$ is less than the proportional limit stress, $\sigma^k_{pl}$, no more calculations are performed for the $k$th layer in this iteration. If $\bar{\sigma}^k > \sigma^k_{pl}$, the effective strain $\bar{e}^k$ is

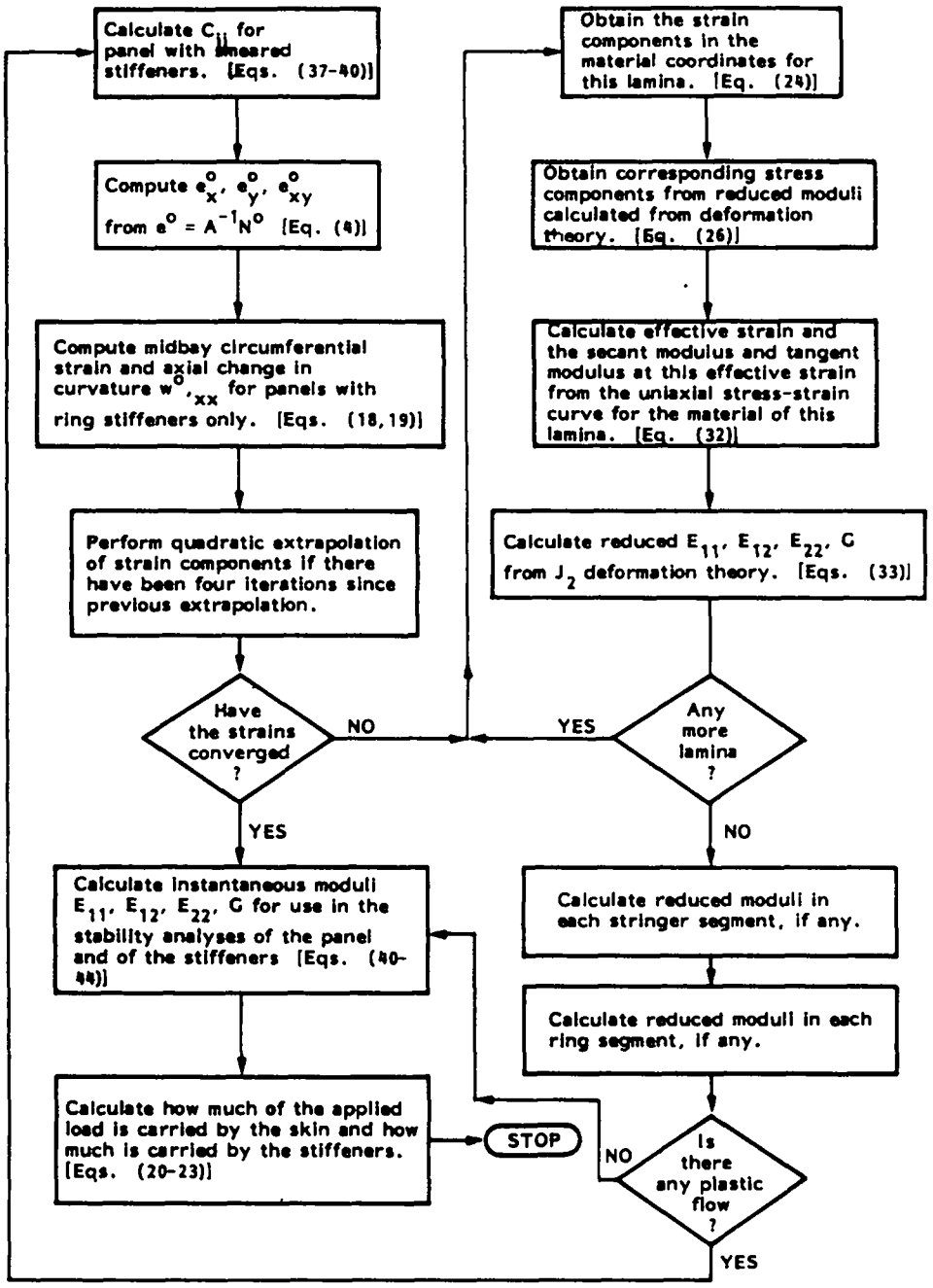


Fig. 7. Flow of calculations for elastic–plastic prebuckling analysis in PANDA.

computed from:

$$\bar{e}^k = 0.4714[(e_1^k - e_2^k)^2 + (e_1^k - e_3^k)^2 + (e_2^k - e_3^k)^2 + 3(e_{12}^k)^2/2]^{1/2}. \quad (28)$$

The strain $e_3^k$ normal to the reference surface is calculated from:

$$e_3^k = -(e_1^k + e_2^k)(\nu + g/3)(1 - \nu + g/3) \quad (29)$$

in which:

$$g = 1.5(E^k/E_s^k - 1) \quad (30)$$

where $E_s^k$ is the secant modulus obtained from the previous iteration. The effective strain $\bar{e}^k$ is compared with $\bar{e}_I^k$, where:

$$\bar{e}_I^k = e_I^k - (1 - 2\nu)\sigma_I^k/(3E^k). \quad (31)$$

In eqn (31) $e_I$ and $\sigma_I$ are coordinates of the stress–strain curve for the material of the $k$th layer. These are provided by the user of PANDA. The values of $e_I^k$ and $\sigma_I^k$ that lie on the stress–strain curve and produce $\bar{e}_I^k$ equal to $\bar{e}^k$ from eqn (28) are used to determine new estimates of the tangent and secant

moduli $E_T^k$ and $E_s^k$, respectively:

$$E_T^k = \mathrm{d}\sigma_j^k/\mathrm{d}e_j^k; \quad E_s^k = \sigma_j^k/e_j^k. \tag{32}$$

The new estimate of the effective stress is, of course, $\sigma_j^k$. In PANDA the stress–strain curve is represented in a piecewise linear fashion, the linear segments connecting coordinates $(e_j, \sigma_j)$, $j = 1, 2, \ldots$ that are supplied by the program user. A smoothing technique is used in the determination of $E_T^k$ in order to prevent oscillatory behavior in the optimization phase associated with corners between line segments of the stress–strain curve.

New values of the moduli $E_{11}^k$, $E_{12}^k$, $E_{22}^k$ and $G^k$ are computed from $J_2$-deformation theory [6]:

$$\begin{aligned} E_{11}^k &= a/\Delta \\ E_{22}^k &= E_{11}^k \\ E_{12}^k &= b/\Delta \\ G^k &= G_e^k(1+\nu)/(1+\nu+g) \end{aligned} \tag{33}$$

in which $G_e^k$ is the elastic shear modulus of the $k$th layer and

$$a \equiv (1 + 2g/3)/E^k \tag{34a}$$

$$b \equiv (\nu + g/3)/E^k \tag{34b}$$

$$g \equiv 1.5(E^k/E_s^k - 1) \tag{34c}$$

$$\Delta \equiv a^2 - b^2. \tag{34d}$$

The above calculations are repeated for every layer in the laminate.

The reduced moduli of the stiffener segments are determined in a completely analogous fashion, except that the effective strain [eqn (28)] is replaced by

$$\bar{e} = e_x^0 \tag{35}$$

for all stringer segments and

$$\bar{e} = (R/R_{c.g.})e_{y\,\mathrm{skin}}^0 (x = a_0/2) \tag{36}$$

for all ring segments. The quantity $R_{c.g.}$ is the radius to the ring centroid and $e_{y\,\mathrm{skin}}^0(x = a_0/2)$ is the strain in the skin at the ring attachment point [eqn (19b)].

*Integrated constitutive law.* The integrated constitutive law for the laminated panel skin, for both the prebuckling analysis and the stability analysis, has the form:

$$\begin{Bmatrix} N_x \\ N_y \\ N_{xy} \\ M_x \\ M_y \\ M_{xy} \end{Bmatrix} = \left[\begin{array}{ccc:ccc} A_{11} & A_{12} & A_{16} & B_{11} & B_{12} & B_{16} \\ A_{12} & A_{22} & A_{26} & B_{12} & B_{22} & B_{26} \\ A_{16} & A_{26} & A_{66} & B_{16} & B_{26} & B_{66} \\ \hdashline B_{11} & B_{12} & B_{16} & D_{11} & D_{12} & D_{16} \\ B_{12} & B_{22} & B_{26} & D_{12} & D_{22} & D_{26} \\ B_{16} & B_{26} & B_{66} & D_{16} & D_{26} & D_{66} \end{array}\right] \begin{Bmatrix} e_x \\ e_y \\ e_{xy} \\ \kappa_x \\ \kappa_y \\ 2\kappa_{xy} \end{Bmatrix} = \mathbf{Ce} \tag{37}$$

in which $N_x, N_y, \ldots M_{xy}$ are the stress and moment resultants and $e_x, e_y, \ldots \kappa_{xy}$ are the reference surface strains, changes in curvature, and twist. The $A_{ij}$, $B_{ij}$ and $D_{ij}$ are given by Jones [7]:

$$\begin{aligned} A_{ij} &= \sum_{k=1}^{NL} (\bar{Q}_{ij})_k (z_k - z_{k-1}) \\ B_{ij} &= \frac{1}{2}\sum_{k=1}^{NL} (\bar{Q}_{ij})_k (z_k^2 - z_{k-1}^2) \\ D_{ij} &= \frac{1}{3}\sum_{k=1}^{NL} (\bar{Q}_{ij})_k (z_k^3 - z_{k-1}^3) \end{aligned} \tag{38}$$

in which the $z_k$ are measured from the reference surface. The $\bar{Q}_{ij}$ for each lamina are given by Jones as:

$$\begin{aligned} \bar{Q}_{11} &= E_{11}c^4 + 2(E_{12} + 2G)s^2c^2 + E_{22}s^4 \\ \bar{Q}_{12} &= (E_{11} + E_{22} - 4G)s^2c^2 + G(s^4 + c^4) \\ \bar{Q}_{22} &= E_{11}s^4 + 2(E_{12} + 2G)s^2c^2 + E_{22}c^4 \\ \bar{Q}_{16} &= (E_{11} - E_{12} - 2G)sc^3 + (E_{12} - E_{22} + 2G)s^3c \\ \bar{Q}_{26} &= (E_{11} - E_{12} - 2G)s^3c + (E_{12} - E_{22} + 2G)sc^3 \\ \bar{Q}_{66} &= (E_{11} + E_{22} - 2E_{12} - 2G)s^2c^2 + G(s^4 + c^4). \end{aligned} \tag{39}$$

For the prebuckling phase, $E_{11}$, $E_{12}$, $E_{22}$ and $G$ are the reduced moduli defined in eqns (33), $c$ and $s$ are defined in eqn (25), and $\phi$ is the angle from the axial direction to the fiber axis of the lamina (direction in which the modulus $E_1$ is measured (Fig. 2)).

*"Smeared" stiffeners.* For the calculation of the average prebuckling strain components from eqn (4), the stiffeners must be treated as part of the skin, that is, "smeared out" over the panel surface. This "smearing" is accomplished via a theory used by Baruch and Singer [8] as described in the text by Brush and Almroth [9]. To certain of the constitutive coefficients $A_{ij}$, $B_{ij}$ and $D_{ij}$ in eqn (37) are added terms that reflect the extensional, bending and torsional rigidities of the rings and stringers. For example, with external rings and external stringers (positive eccentricities), all of the segments which are of the same material, new constitutive coefficients $C_{ij}$ are obtained as follows:

$$\begin{aligned} C_{11} &= A_{11} + E_s^s A^s/b_0 \\ C_{22} &= A_{22} + E_s^r A^r/a_0 \\ C_{14} &= B_{11} + e^s E_s^s A^s/b_0 \end{aligned}$$

$$C_{25} = B_{22} + e^r E_s^r A^r/a_0$$
$$C_{44} = D_{11} + E_s^s I^s/b_0$$
$$C_{55} = D_{22} + E_s^r I^r/a_0$$
$$C_{66} = D_{66} + (\bar{G}^s J^s/b_0 + \bar{G}^r J^r/a_0)/4 \qquad (40)$$

in which superscripts $s$ and $r$ denote "stringer" and "ring", respectively; subscript $s$ denotes "secant modulus"; $\bar{G}$ is the effective elastic–plastic shear modulus:

$$\bar{G} = G_e(1+\nu)/(1+\nu+g) \qquad (41)$$

with $g$ given by eqn (34c); and $J$ is the torsion constant for the stiffener cross-section. The quantities $e^s$ and $e^r$ are the distances from the skin reference surface to the centroidal axes of the stringers and rings, respectively, positive when these axes lie on the outside of the shell.

The new prebuckling $C_{ij}$ in eqn (40) are used to calculate new average strain components from eqn (4), as indicated in Fig. 7. Equations (5)–(41) are solved again. Iterations continue until the prebuckling strain components $e_x^0$, $e_{y\text{skin}}^0$, $e_{xy}^0$ change no more than 0.01% from their values as of the previous iteration. Figure 8 shows the results of several prebuckling iterations applied to a ring-stiffened submarine hull subject to uniform external hydrostatic compression. Quadratic extrapolation of the strain components is used every four iterations.

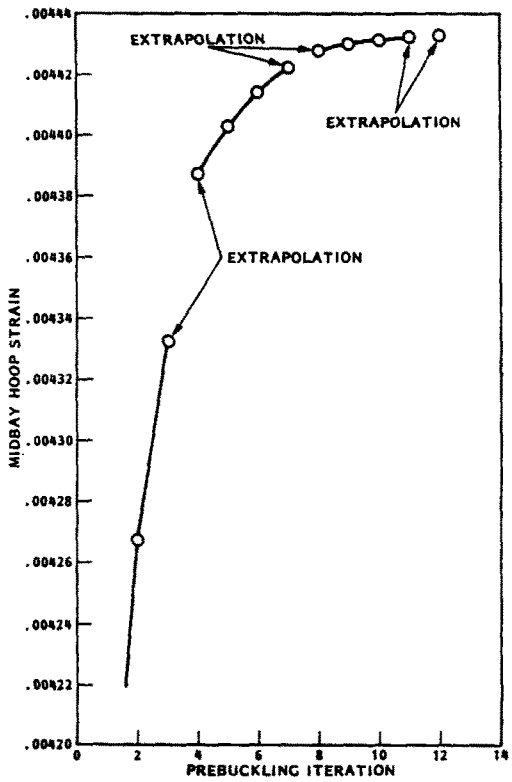


Fig. 8. Typical convergence of the prebuckling strain in the plastic region. This case corresponds to a hydrostatically compressed, ring-stiffened cylindrical shell.

*Instantaneous moduli for stability analysis.* Once convergence of the prebuckling strain components has been achieved, the instantaneous moduli (tangent moduli) governing stability are calculated. The instantaneous moduli for the $k$th layer of the panel skin can be calculated with use of $J_2$-deformation theory [6]:

$$E_{11b}^k = a/\Delta$$
$$E_{12b}^k = b/\Delta$$
$$E_{22b}^k = c/\Delta$$
$$G_b^k = G_e^k(1+\nu)/[1+\nu+g+2g'(\sigma_{12}^k)^2] \qquad (42)$$

in which:

$$a \equiv (1 + 2g/3 + g's_2^2)/E^k$$
$$b \equiv (\nu + g/3 - g's_1 s_2)/E^k$$
$$c \equiv (1 + 2g/3 + g's_1^2)/E^k$$
$$\Delta \equiv ac - b^2 \qquad (43)$$

with $g$ given by eqn (34c),

$$g' = 2.25E^k(1/E_T^k - 1/E_s^k)/\bar{\sigma}^2 \qquad (44)$$

and the stress deviators $s_1$ and $s_2$ given by:

$$s_1 = (2\sigma_1^k - \sigma_2^k)/3 \quad s_2 = (2\sigma_2^k - \sigma_1^k)/3. \qquad (45)$$

Analogous formulas are used for the instantaneous moduli of the stiffener segments. The instantaneous moduli given in eqn (42) are used in eqns (39), which, through eqns (38), yield new coefficients $A_{ij}^b$, $B_{ij}^b$ and $D_{ij}^b$ in eqn (37), that apply during the buckling phase of the analysis. Superscript $b$ denotes "value during buckling modal deformation".

For the calculation of general instability and "semi-general" instability, at least one set of stiffeners must be smeared out over whatever domain within the panel $[(a, b), (a_0, b), (a, b_0)]$ is being considered during the current buckling analysis. Formulas for the instantaneous stiffness coefficients $C_{ij}^b$ are similar to those given for $C_{ij}$ in eqn (40), with the secant moduli $E_s^s$, $E_s^r$ for the stringers and rings being replaced by the tangent moduli $E_T^s$, $E_T^r$, and the $A_{ij}$, $B_{ij}$, $D_{ij}$ being replaced by $A_{ij}^b$, $B_{ij}^b$, $D_{ij}^b$.

### *General, "semi-general" and local instability of panel*

*Governing equations.* For layered and stiffened shells with membrane-bending coupling, eqns (37), as modified in accordance with eqns (40), (42), may be written in the form:

$$\begin{Bmatrix} N^b \\ M^b \end{Bmatrix} = \begin{bmatrix} A & B \\ B & D \end{bmatrix} \begin{Bmatrix} e^b \\ \kappa^b \end{Bmatrix} = {}^{6\times 6}\mathbf{C}\,\mathbf{e}^b \qquad (46)$$

where superscript $b$ denotes "value due to buckling modal deformation"; $A$, $B$, and $D$ are $3 \times 3$ symmetric full matrices containing the instantaneous stiffness coefficients just derived (superscript $b$ dropped for convenience); and

$$\lfloor N^b; M^b \rfloor \equiv \lfloor N^b_x, N^b_y, N^b_{xy}; M^b_x, M^b_y, M^b_{xy} \rfloor$$

$$\lfloor e^b; \kappa^b \rfloor \equiv \lfloor e^b_x, e^b_y, e^b_{xy}; \kappa^b_x, \kappa^b_y, 2\kappa^b_{xy} \rfloor = \mathbf{e}^b. \quad (47)$$

The strain energy $U$ and work $W$ done by the prebuckling in-plane loads $N^0_x$, $N^0_y$, $N^0_{xy}$ during the buckling process are given by:

$$U = \frac{1}{2}\int_0^{y_{max}}\int_0^{x_{max}} \mathbf{e}^{bT}\mathbf{C}\mathbf{e}^b \, dx \, dy \quad (48)$$

$$W = \frac{1}{2}\int_0^{y_{max}}\int_0^{x_{max}} (N^0_x w^{b2}_{,x} + N^0_y w^{b2}_{,y} + 2N^0_{xy} w^b_{,x} w^b_{,y}) \, dx \, dy \quad (49)$$

in which the upper limits of integration $x_{max}$ and $y_{max}$ depend on what kind of instability is being investigated, general, "semi-general" or local, as follows:

| Type of instability | $x_{max}$ | $y_{max}$ |
|---|---|---|
| General | $a$ | $b$ |
| Between rings, smeared stringers | $a_0$ | $b$ |
| Between stringers, smeared rings | $a$ | $b_0$ |
| Local | $a_0$ | $b_0$ |

In the domains $(x, y)$ bounded by $(a, b)$ or $(a_0, b)$ or $(a, b_0)$ or $(a_0, b_0)$, the buckling modal displacement components $u^b$, $v^b$, $w^b$ are assumed to have the general form:

$$u^b = A(n_2^2 m_1 \sin(n_1 y - m_1 x) + n_1^2 m_2 \sin(n_2 y + m_2 x))$$

$$v^b = B(n_2 \sin(n_1 y - m_1 x) - n_1 \sin(n_2 y + m_2 x))$$

$$w^b = C(\cos(n_1 y - m_1 x) - \cos(n_2 y + m_2 x)) \quad (50)$$

in which:

$$n_1 = n + mc \quad m_1 = m + nd$$
$$n_2 = n - mc \quad m_2 = m - nd. \quad (51)$$

The displacement functions (50) were chosen to permit nearly inextensional reference surface buckling strain components, $e^b_x$, $e^b_y$ and $e^b_{xy}$, and to allow reasonably accurate determination of buckling loads in the presence of shear and unbalanced laminates without the need for series expansions. The wave indices $n$ and $m$ are:

$$n \equiv \bar{n}\pi/y_{max} \quad m \equiv \bar{m}\pi/x_{max} \quad (52)$$

in which the quantities $\bar{m}$ and $\bar{n}$ are the numbers of half-waves over the arc lengths $x_{max}$ and $y_{max}$, respectively. The reference surface buckling strains and changes in curvature from Donnell's theory [3] are given by:

$$e^b_x = u^b_{,x}$$
$$\kappa^b_x = -w^b_{,xx}$$
$$e^b_y = v^b_{,y} + w^b/R$$
$$\kappa^b_y = -w^b_{,yy}$$
$$e^b_{xy} = u^b_{,y} + v^b_{,x}$$
$$\kappa^b_{xy} = -w^b_{,xy} \quad (53)$$

where $(\,)_{,x}$ and $(\,)_{,y}$ indicate differentiation.

Insertion of eqns (50) into eqns (53) and (48), (49) leads to an expression for the total potential energy, $U - W$, of the form:

$$U - W = [A, B, C]\begin{bmatrix} a_{11} & a_{12} & a_{13} \\ a_{12} & a_{22} & a_{23} \\ a_{13} & a_{23} & a_{33} \end{bmatrix}\begin{Bmatrix} A \\ B \\ C \end{Bmatrix} \quad (54)$$

in which:

$$a_{11} = C_{11}(n_2^4 m_1^4 + n_1^4 m_2^4) + C_{33}(n_2^4 n_1^2 m_1^2 + n_1^4 n_2^2 m_2^2) + \underline{2C_{13}(-n_2^4 m_1^3 n_1 + n_1^4 m_2^3 n_2)} \quad (55a)$$

$$a_{12} = (C_{12} + C_{33})(n_2^3 n_1 m_1^2 + n_1^3 n_2 m_2^2) + C_{13}(n_2^3 m_1^3 - n_1^3 m_2^3) + \underline{C_{23}(n_2^3 n_1^2 m_1 - n_1^3 n_2^2 m_2)} \quad (55b)$$

$$a_{22} = 2C_{22} n_1^2 n_2^2 + C_{33}(n_2^2 m_1^2 + n_1^2 m_2^2) + \underline{2C_{23}(-n_1 n_2^2 m_1 + n_1^2 n_2 m_2)} \quad (55c)$$

$$a_{13} = -C_{12}(n_2^2 m_1^2 + n_1^2 m_2^2)/R - C_{14}(n_2^2 m_1^4 + n_1^2 m_2^4) - (C_{15} + 2C_{36}) n_1^2 n_2^2 (m_1^2 + m_2^2) + \underline{(2C_{16} + C_{34})(n_2^2 n_1 m_1^3 - n_1^2 n_2 m_2^3)} + \underline{C_{23}(n_2^2 n_1 m_1 - n_1^2 n_2 m_2)/R} + \underline{C_{35}(n_2^2 n_1^3 m_1 - n_1^2 n_2^3 m_2)} \quad (55d)$$

$$a_{23} = n_1 n_2 [2C_{22}/R + (C_{24} + 2C_{36})(m_1^2 + m_2^2) + C_{25}(n_1^2 + n_2^2)] + \underline{(2C_{26} + C_{35})(-n_1^2 n_2 m_1 + n_2^2 n_1 m_2)} + \underline{C_{23}(-n_2 m_1 + n_1 m_2)/R} + \underline{C_{34}(-n_2 m_1^3 + n_1 m_2^3)} \quad (55e)$$

$$
\begin{aligned}
a_{33} = {} & 2C_{22}/R^2 + 2C_{24}(m_1^2 + m_2^2)/R \\
& + 2C_{25}(n_1^2 + n_2^2)/R \\
& + C_{44}(m_1^4 + m_2^4) + C_{55}(n_1^4 + n_2^4) \\
& + (2C_{45} + 4C_{66})(n_1^2 m_1^2 + m_2^2 n_2^2) \\
& + N_{XPRE}(m_1^2 + m_2^2) + N_{YPRE}(n_1^2 + n_2^2) \\
& + 2N_{XYPRE}(n_2 m_2 - n_1 m_1) \\
& + \underline{4C_{26}(-n_1 m_1 + n_2 m_2)/R} \\
& + \underline{4C_{46}(-n_1 m_1^3 + n_2 m_2^3)} \\
& + \underline{4C_{56}(-n_1^3 m_1 + n_2^3 m_2)}. \qquad (55f)
\end{aligned}
$$

In eqns (55), the $C_{ij}$ are coefficients of the integrated constitutive law C relating buckling modal stress and moment resultants to buckling modal reference surface strains and changes in curvature [eqns (37), (40), (46)]. $N_{XPRE}$, $N_{YPRE}$, and $N_{XYPRE}$ are in-plane loads that are not multiplied by the load factor (eigenvalue) $\lambda$, but represent a fixed prestressed state. The total prebuckling in-plane load components, $N_x^0$, $N_y^0$, $N_{xy}^0$, which appear in eqn (49) are given by:

$$N_x^0 = N_{XPRE} + \lambda N_{xe} \qquad (56a)$$

$$N_y^0 = N_{YPRE} + \lambda N_{ye} \qquad (56b)$$

$$N_{xy}^0 = N_{XYPRE} + \lambda N_{xye} \qquad (56c)$$

in which $\lambda$ is a load factor to be calculated in the buckling analysis and subscript "$e$" denotes "eigenvalue parameter". One finds the eigenvalue $\lambda$ by setting the determinant of the $a$-matrix on the right-hand-side of eqn (54) equal to zero. The resulting expression for $\lambda$ is:

$$\lambda = \frac{a_{33} + \dfrac{[a_{23}(a_{12}a_{13} - a_{11}a_{23}) + a_{13}(a_{12}a_{23} - a_{13}a_{22})]}{(a_{11}a_{22} - a_{12}^2)}}{-N_{xe}(m_1^2 + m_2^2) - N_{ye}(n_1^2 + n_2^2) - 2N_{xye}(m_2 n_2 - m_1 n_1)}. \qquad (57)$$

The constraint imposed on the design during the optimization process is that $\lambda$ should be greater than unity. Equations (46)–(57) apply to any kind of shell buckling: general, "semi-general" or local. The load factors $\lambda$ corresponding to the various types of instability are calculated with use of appropriate $C_{ij}$, $x_{max}$ and $y_{max}$ pertaining to whatever portion of the structure is being investigated. For general instability both rings and stringers are smeared out; for "semi-general" buckling, either rings or stringers are smeared out; and, for local skin buckling, neither set of stiffeners is smeared out. All buckling load multipliers $\lambda$ are calculated with the assumptions that the boundaries of the portion of the structure under investigation are simply supported. Note that the simple-support condition is violated if either $c$ or $d$ in eqns (51) are not equal to zero.

The expression for $\lambda$ contains unknown quantities $m$, $n$, $c$ and $d$. When in-plane shear $N_{xy}^0$ is present or when any of the terms $A_{i6}$, $B_{i6}$, $D_{i6}$, $i \neq 6$ [see eqn (37)] is non-zero, the minimum value of $\lambda$ for fixed $m$ and $n$ with respect to the slope, $c$ or $d$, of the blocking nodal lines is found. In the calculation of this minimum it is always assumed that either $c$ or $d$ is zero. Figure 9 shows the model. For each kind of buckling, general, semi-general or local, a test is made to see in which coordinate direction the panel is "long". The test is based on the quantity

$$\bar{L} = (x_{max}/y_{max})(C_{55_N}/C_{44_N})^{1/2} \qquad (58)$$

in which $C_{ii_N}$ are the bending stiffnesses referred to the neutral axes in the $x$- and $y$-directions. If the panel is shallow ($R/y_{max} > 1.0$) and if $\bar{L} \geq 1.0$, the panel is effectively "long" in the $x$-direction and the model shown in Fig. 9(a) is used. If the panel is not shallow ($R/y_{max} < 1.0$) or if $\bar{L} < 1$, the opposite is true and the model shown in Fig. 9(b) is used. In this way, the boundary conditions are satisfied along the edges that span the least number of buckling modal half-waves while the correct solution is obtained for buckling of a long cylinder under pure torsion. The boundaries along which the simple support conditions are violated span the largest number of half-waves and hence the conditions there least affect the critical load. The utility of the approximate expressions (50) is thereby maximized. Such a strategy is advantageous because the buckling loads must be calculated very often in the optimization analysis. Since the optimum design is being obtained interactively, it is necessary to avoid discouraging or boring the program user by making him wait a long time at the terminal while elaborate buckling calculations proceed for each new trial design.

To increase the efficiency of the subroutine that calculates buckling loads, the terms in eqns (55) are arranged so that those which are often zero [e.g. the terms underlined in eqns (55)] are not calculated if it is known in advance that they are zero.

The eigenvalue is modified by a factor "DONNEL" $= (n_c^2 - 1)/n_c^2$ under certain conditions for which the Donnell theory [eqns (49), (53)] yields inaccurate results, such as buckling of a complete cylindrical shell under uniform external pressure for which $n_{cr}$ is less than 4 or 5 half-waves over 180° of the circumference. The factor "DONNEL" is not applied if $n_c = 1$ or if the axial half-wavelength of the buckling pattern is less than the radius $R$ of the cylinder, or if the loading is predominately axial ($N_{x0} > N_{y0}$).

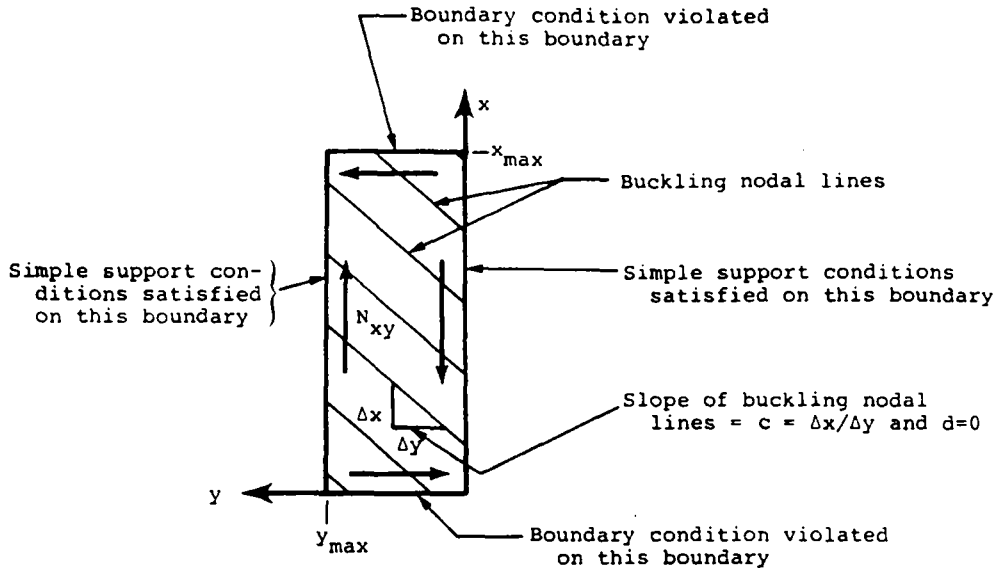


(a) Assumed buckling mode for panel that is "long" in the x-direction: $w = C \sin(ny)\sin[m(x-cy)]$

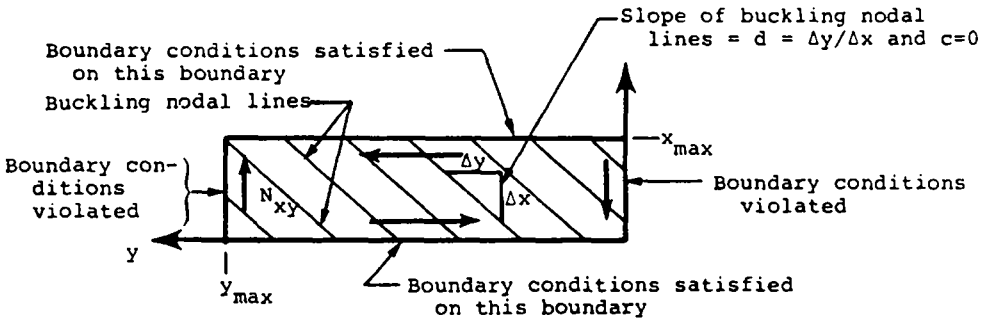


(b) Assumed buckling mode for panel that is "long" in the y-direction: $w = \sin[n(y-dx)]\sin(mx)$

Fig. 9. Assumed buckling modal patterns with shear and/or unbalanced laminates present.

*Strategy for finding the minimum buckling load with respect to* $\bar{m}$, $\bar{n}$, c *or* d. For each wave index combination, $\bar{m}$ and $\bar{n}$, the minimum $\lambda$ with change in the buckling nodal line slope $c$ or $d$ is found (only in cases for which shear loading is present or any $A_{i6}$, $B_{i6}$ or $D_{i6} \neq 0$; $i \neq 6$) by variation of $c$ or $d$ in equal increments or decrements of 0.01 if its absolute value is less than 0.1 and by a factor of 1.2 if its absolute value is greater than 0.1. The buckling nodal line slopes are shown in Fig. 9.

The minimum $\lambda$ with respect to the wave indices $\bar{m}$ and $\bar{n}$ is found with due attention to the fact that for a given geometry and loading this minimum may be non-unique, as pointed out by Burns [10] and by Pappas and Allentuch [11]. Four regions in $(\bar{m}, \bar{n})$ space are searched for minima in the function $\lambda(\bar{m}, \bar{n})$: low $\bar{m}$, low $\bar{n}$; low $\bar{m}$, high $\bar{n}$; high $\bar{m}$, low $\bar{n}$; and high $\bar{m}$, high $\bar{n}$. Figure 10 shows the results of such a search for an axially compressed composite unstiffened cylindrical shell, the dimensions and properties of which are taken from Booton and Tennyson's paper [12].

For low $\bar{m}$ ($\bar{m} = 1$), the search begins at:

$$\bar{n}_{start_1} = (y_{max}/x_{max})(C_{44}/C_{55})^{1/4} \quad \text{or} \quad \bar{n}_{start_1} = 1, \quad (59)$$

whichever is larger. With $\bar{m} = 1$, a minimum $\lambda(1, \bar{n})$ is sought. The region in $(\bar{n}, \bar{m})$ space surrounding this minimum is then explored by variation of both $\bar{m}$ and $\bar{n}$. When a local minimum $\lambda_1(\bar{m}_{L1}, \bar{n}_{L1})$ has been found, $\bar{m}$ is reset to unity and a new minimum $\lambda_1(1, \bar{n})$ is sought in whichever region was not covered by the initial search that began at $\bar{n}_{start}$ given by eqn (59). If the minimum $\bar{n}$ covered in the search for $\lambda_1(\bar{m}_{L1}, \bar{n}_{L1})$ is greater than or equal to 3, the low-$\bar{n}$ range is next covered, starting at $\bar{n} = 1$. If the low-$\bar{n}$ range was

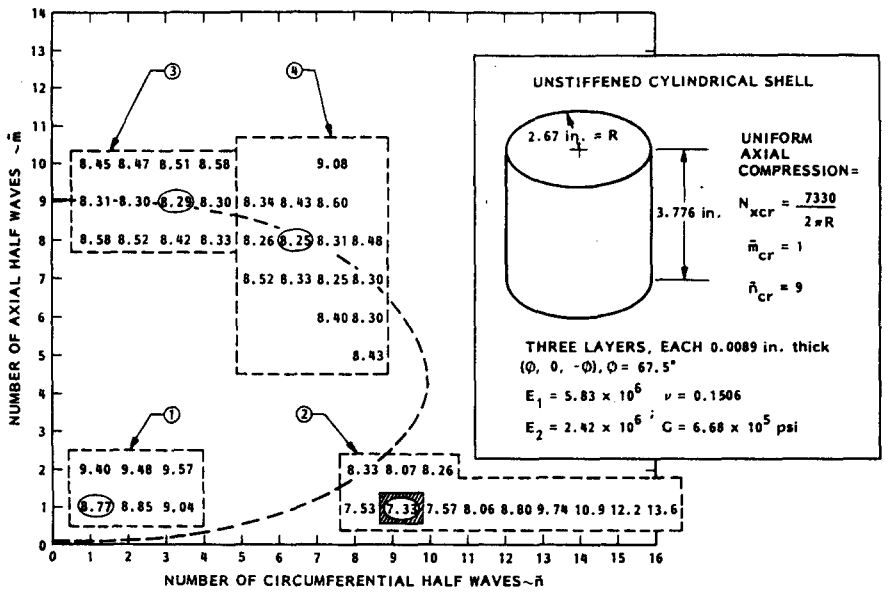


Fig. 10. Buckling loads for axially compressed composite cylindrical shell with an unbalanced laminate $(\phi, 0, -\phi)$. Four regions, 1, 2, 3, 4, are shown in which minimum critical load multipliers $\lambda_{cr}$ $(\bar{m}_{cr}, \bar{n}_{cr})$ are sought. The numbers in the dashed boxes are buckling loads in thousands of pounds for each $(\bar{m}, \bar{n})$ combination investigated by PANDA.

covered in the search for $\lambda_1(\bar{m}_{L1}, \bar{n}_{L1})$, the high-$\bar{n}$ range is next covered, starting at:

$$\bar{n}_{start_2} = y_{max}/(0.2\,R). \tag{60}$$

As before, a minimum $\lambda_2(1, \bar{n})$ is sought, after which the region in $(\bar{m}, \bar{n})$ space about this minimum is explored as before in order to find $\lambda_2(\bar{m}_{L2}, \bar{n}_{L2})$, in which subscript $L$ again denotes "local minimum".

For high $\bar{m}$, low $\bar{n}$, the search for $\lambda_3(\bar{m}_{L3}, \bar{n}_{L3})$ begins at $\bar{n} = 1$ and $\bar{m}$ equal to the larger of the following:

$$\bar{m}_{start} = x_{max}/[\pi(R^2 C_{44_N}/C_{22})^{1/4}] \tag{61}$$

or

$$\bar{m} = (x_{max}/y_{max})(C_{55_N}/C_{44_N})^{1/4}. \tag{62}$$

Equation (61) yields approximately the number of axial waves in a cylinder of length $x_{max}$ which buckles axisymmetrically and eqn (62) yields approximately the number of axial waves in an axially compressed flat plate of aspect ratio $x_{max}/y_{max}$. During the search process $\bar{n}$ is increased monotonically. For each $\bar{n}$ a minimum $\lambda_3(\bar{m}, \bar{n})$ is found, eventually leading to $\lambda_3(\bar{m}_{L3}, \bar{n}_{L3})$. The final region, high $\bar{m}$, high $\bar{n}$, is searched for a local minimum $\lambda_4(\bar{m}_{L4}, \bar{n}_{L4})$ starting with:

$$\bar{m}_{start_2} = \bar{m}_{L3} \quad \bar{n}_{start_3} = y_{max}/(0.4R). \tag{63}$$

In Figure 10, the four regions searched are outlined in dashed boxes. It turns out that in this case each of the four regions contains a local minimum load multiplier $\lambda$. PANDA selects the lowest of these minima as the critical load multiplier. In this case, $\lambda_{cr} = \lambda_2(\bar{m}_{L2}, \bar{n}_{L2}) = \lambda_2(1, 9) = 7.33$. The dotted curve in Fig. 10 represents constant values of the quantity:

$$[(\bar{m}\pi R/x_{max})^2 + \bar{n}^2]^2/(\bar{m}\pi R/x_{max})^2 \tag{64}$$

which appears in eqns (5.50) and (5.51) of Brush and Almroth [9]. In the context of Donnell's theory, minimization of the axial buckling load of an isotropic monocoque cylindrical shell with respect to this quantity yields the formula:

$$\frac{P_{cr}}{2\pi R} = \frac{Et^2/R}{[3(1-\nu^2)]^{1/2}} \tag{65}$$

in which $P_{cr}$ is the total critical axial load on the cylinder.

If the quantity (64) is set equal to its value corresponding to the minimum $\lambda(\bar{m}, \bar{n})$ along the $\bar{m}$-axis in Fig. 10 [$\bar{m} = 9$, $\bar{n} = 0$, value of quantity (64) = 400] then the dashed curve in Fig. 10 is obtained for the various $(\bar{m}, \bar{n})$ combinations that yield this same value, 400. It is seen that the dashed curve passes close to all of the minima found by PANDA in $(\bar{n}, \bar{m})$ space.

In the optimization analysis it is necessary not only to find the various buckling loads (local, semi-general, general) at a given design point, but also to determine how these loads vary with a small change in each decision variable from this design point. In PANDA the small change is equal to 5.0% of the current value of the decision variable. Much computer time is saved by use of whatever values of $\bar{m}$, $\bar{n}$, $c$ and $d$ exist at the design point for calculation of the eigenvalue $\lambda$ at these neighboring points also.

*Local buckling (crippling) of stiffener segments*

There are two types of stiffeners, those along cylinder generators called stringers and those along circumferences called rings (Fig. 1). Each type of stiffener is assumed to consist of an assemblage of rectangular pieces of width $b_i$ and thickness $t_i$. The rectangular pieces of each stiffener type are divided into two classes: those that are "internal" or "interior" and those that are "ends". Figure 4 shows examples. "Internal" stiffener segments are those which have both edges connected to other stiffener segments or the panel skin. "Ends" are stiffener segments only one edge of which is connected to another structural part. All stiffener segments are assumed to be flat and long compared to their widths. Thus, for stringers $a_0 \gg b_i^s$ and for ring segments $b_0 \gg b_i^r$. The curvatures of the ring segments are neglected.

*Effective stiffener segment material properties.* The theory for crippling of stiffener segments is based on the assumption that these segments are monocoque and orthotropic, not layered anisotropic. Thus, the terms in eqn (37), $A_{i6}$ and $D_{i6}$; $i \neq 6$, are assumed to be zero and all of the $B_{ij}$ are assumed to be zero when applied to the crippling or rolling analyses of stiffener segments. The PANDA$_1$ program allows the user to provide input as if the stiffener segments were layered anisotropic. From initial values of $A^i_{11}$, $A^i_{12}$, $A^i_{22}$ and $A^i_{66}$ computed from the anisotropic theory for the $i$th stiffener segment laminate corresponding to the user's starting design, effective moduli and Poisson's ratio are derived from:

$$E_{11}^{i(\text{eff})} = A^i_{11}/t^i$$

$$\nu_{12}^{i(\text{eff})} = A^i_{12}/A^i_{22}$$

$$E_{22}^{i(\text{eff})} = A^i_{22}/t^i$$

$$G^{i(\text{eff})} = A^i_{66}/t^i \tag{66}$$

in which:

$$t^i = \sum_{k=1}^{N} t^i_k. \tag{67}$$

During the optimization phase the total thickness $t^i$ of the $i$th stiffener segment laminate may be a decision variable; the thicknesses of each lamina are not decision variables. If the stiffener material is isotropic and if $t^i = t^i_k$ ($N = 1$ layer), the effect of nonlinear material behavior is included in the analysis. The $A^i_{jk}$ in eqn (66) are the instantaneous coefficients referred to in the discussion associated with eqns (42)–(45).

*Local buckling of "internal" segments.* For "internal" segments the critical load factors $\lambda_i$ can be calculated from eqns (55)–(57) with $c = d = N^0_{xy} = N^0_y = 0$, $R \to \infty$, and the "anisotropic" $C^i_{ij} = 0$. The axial prebuckling resultant in eqn (56a) $[N^0_x]$ is interpreted to mean the prebuckling stress resultant along the axis of the stiffener and the wave index $m_1$ is given by $m_i = \bar{m}_i \pi / l$ in which $\bar{m}_i$ is the number of half-waves along $l$, where $l$ is $a_0$ for a stringer segment and $b_0$ for a ring segment. With these simplifications and definitions the terms $a_{13}$ and $a_{23}$ in eqns (55) vanish and eqn (57) becomes:

$$\lambda_i = \frac{[C^i_{44}m_i^2 + C^i_{55}(n_i^4/m_i^2) + (2C^i_{45} + 4C^i_{66})n_i^2 + N^i_{XPRE}]}{-N^i_{xe}}. \tag{68}$$

If it is assumed that the internal stiffener segment buckles with one-half wave ($\bar{n}_i = 1$) across its width $b_i$, as shown in Fig. 5, then it can be shown that:

$$m_i = n_i(C^i_{55}/C^i_{44})^{1/4} = (\pi/b_i)(C^i_{55}/C^i_{44})^{1/4}. \tag{69}$$

The quantities $C^i_{44}$, $C^i_{55}$, $C^i_{45}$ and $C^i_{66}$ in eqns (68), (69) are given by:

$$C^i_{44} = E_{11}^{i(\text{eff})} t^{i3}/12$$

$$C^i_{45} = \nu_{12}^{i(\text{eff})} E_{11}^{i(\text{eff})} t^{i3}/12$$

$$C^i_{55} = E_{22}^{i(\text{eff})} t^{i3}/12$$

$$C^i_{66} = G^{i(\text{eff})} t^{i3}/12. \tag{70}$$

Use of eqn (69) with $n_i = \pi/b_i$ in eqn (68) yields:

$$\lambda_i = \frac{\{2(\pi/b_i)^2[(C^i_{44}C^i_{55})^{1/2} + C^i_{45} + 2C^i_{66}] + N^i_{XPRE}\}}{-N^i_{xe}} \tag{71}$$

in which:

$$N^i_{XPRE} \equiv N^i_{\bar{x}pre} \tag{72}$$

$$N^i_{xe} = N^{i0}_{\bar{x}} - N^i_{\bar{x}pre} \tag{73}$$

where $N^{i0}_{\bar{x}}$, given by eqn (20), is the total prebuckling axial resultant (lb/in.) carried by the $i$th stiffener segment and $N^i_{\bar{x}pre}$ is that portion of the prebuckling axial resultant carried by the $i$th stiffener segment that is not to be multiplied by the load factor $\lambda_i$.

*Local buckling of "end" segments.* It is assumed here that the stiffener "end" segment cross-section does not deform in the buckling mode (Fig. 5, Segment 3). The assumed displacement function is:

$$w^i = C\bar{y}_i \sin[\bar{m}^j \pi \bar{x}/l] = C\bar{y}_i \sin[m^j \bar{x}]$$

$$u^i = 0$$

$$v^i = 0. \tag{74}$$

Use of eqns (74) in eqns (48), (49), (53) leads to the following expressions for strain energy of and work done on the $i$th segment:

$$U^i = C^2 \frac{l}{4}[C^i_{44}(m^j)^4 b_i^3/3 + 4C^i_{66}(m^j)^2 b_i] \tag{75}$$

$$W^i = C^2 \frac{l}{4}[N^{0i}_{\bar{x}}(m^j)^2 b_i^3/3]. \tag{76}$$

In eqn (74), $\bar{y}_i$ is the distance along the width of the "end", as shown in Fig. 4, and $\bar{m}^j$ is the number of half-waves in the local critical buckling pattern of the structural segment to which the end segment is attached (Segment $j$). For example, with reference to Fig. 5, for stiffener Segment 3($i = 3, j = 2$), $m^j$ is given by:

$$m^{(j)} = m^{(2)} = (\pi/b_2)[C^{(2)}_{55}/C^{(2)}_{44}]^{1/4}. \quad (77)$$

For blade stiffeners, such as shown in Fig. 4(c):

$$m^j = \bar{m}_{\text{skin}}\pi/l. \quad (78)$$

With the total prestress resultant $N^{0i}_{\bar{x}}$ in the end segment defined by eqn (73), minimization of the total potential energy, $U^i - W^i$, with respect to the undetermined coefficient $C$ in eqns (75), (76) yields the following equation for the buckling load factor $\lambda_i$:

$$\lambda_i = \frac{C^i_{44}(m^j)^2 b_i^3 + 12C^i_{66}b_i + N^i_{\bar{x}pre}b_i^3}{-N^i_{\bar{x}e}b_i^3}. \quad (79)$$

If more than one "end" segment is attached to the same "internal" segment or to the skin, the buckling criterion is:

$$-\sum_{k=1}^{K_e}(N^k_{\bar{x}pre} + \lambda N^k_{\bar{x}e})b_k^3 = \sum_{k=1}^{K_e}[(m^j)^2 C^k_{44}b_k^3 + 12C^k_{66}b_k] \quad (80)$$

in which $K_e$ is the number of "end" segments attached to the $j$th "internal" segment or to the panel skin.

*Rolling modes*

Three types of rolling modes of instability have been described in the summary and are illustrated in Fig. 6. PANDA accounts for these three types of rolling, one [Fig. 6(a)] in which the panel skin participates and two [Figs 6(b), (c)] in which it does not.

*Rolling with participation of the panel skin*

For panels stiffened by both rings and stringers, there are three eigenvalues (buckling load factors $\lambda$) corresponding to the type of rolling in which the panel skin participates. These modes are characterized by: (1) local rolling between rings and stringers, with both sets of stiffeners twisting about nodal lines of the buckling pattern; (2) rolling in which the stringers are smeared out and the rings twist about nodal lines of the buckling pattern; and (3) rolling in which the rings are smeared out and the stringers twist about nodal lines in the buckling pattern.

Figures 11 and 12 show in more detail the geometry of the type of rolling deformation depicted in Fig. 6(a). This deformation is assumed to be either local, that is, the distances $x_{\max}$ and $y_{\max}$ considered in the rolling instability mode are the spacings $a_0$ and $b_0$ between the rings and stringers, respectively, or "semi-general," that is, the distances $x_{\max}$ and $y_{\max}$ apply to subdomains of the structure with either rings or stringers smeared and the opposite set of stiffeners twisting along simply-supported boundaries. The widths of the stiffener segments are assumed to be small compared to the half-wavelength, $l/\bar{m}$, of the rolling buckling modes. For local rolling the quantity $l$ is the distance $a_0$ between rings in the rolling analysis of stringers and $l$ is the distance $b_0$ between stringers in the rolling analysis of rings. All stiffener segments are assumed to be perpendicular or parallel to the plane of the skin. The effect of curvature of the ring segments on cylindrical panels is neglected.

The assumed deflection field given in Fig. 12 leads to zero in-plane shear of each stiffener segment. Although Fig. 11 may seem to imply that the following analysis applies only to stringers, this is not so. It is emphasized that the analysis of this section applies to rings as well. Figure 12 shows the $\bar{x}, \bar{y}, \bar{z}$ coordinate system and associated displacement components, $u^*, v^*, w^*$, and rotation components, $\omega_{\bar{y}}$ and $\omega_{\bar{z}}$.

The rolling deformations depicted in Figs 11 and 12 cause inextensional bending and twisting of the stiffener web and extensional deformation of the flange. The strain energy of the extensional (membrane) deformation of the flange is large compared to its inextensional (bending and twisting) strain energy. Therefore, in the discussion that follows, the inextensional strain energy of the flange is neglected.

*Membrane energy.* That portion of the strain energy of the stiffener associated with membrane-type deformations of the $i$th stiffener segment deforming in the rolling mode is:

$$U^i_m = \frac{1}{2}\int_{\bar{y}_i=0}^{b_i}\int_{\bar{x}=0}^{l} u^{*2}_{\bar{x}}C^i_{11}\,d\bar{x}\,d\bar{y}_i \quad (i \neq \text{web}) \quad (81)$$

in which $\bar{y}_i$ is the local coordinate shown in Fig. 4, $u^*_{\bar{x}}$ is the axial strain in this segment, $C^i_{11}$ is the instantaneous stiffness coefficient [same as $A^i_{11}$ in eqn (66)], $b_i$ is the width of the segment and $l$ is the length of whatever portion of the panel is being investigated, as follows:

| Type of rolling instability | $l$ | Eqn (81) applies to: |
|---|---|---|
| Local stringer | $a_0$ | Stringer energy |
| Local ring | $b_0$ | Ring energy |
| Smeared stringers | $b$ | Ring energy |
| Smeared rings | $a$ | Stringer energy |

The total membrane energy of the stiffener is:

$$U_m \sum_{\substack{i=1 \\ i\neq\text{web}}}^{N} U^i_m \quad (82)$$

[$i \neq$ web or other segments attached along the line $\bar{y} = \bar{z} = 0$ (Fig. 12)]

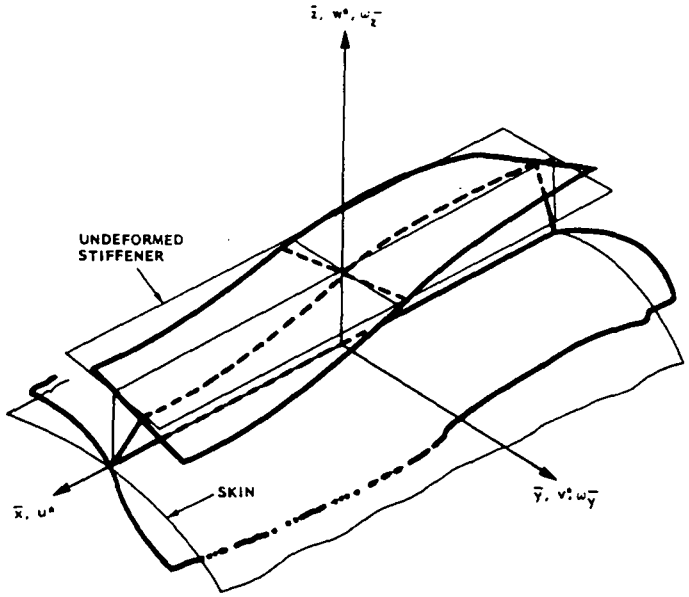


Fig. 11. Rolling of stiffener as in Fig. 6(a).

in which $N$ is the number of segments in the stiffener cross-section.

The corresponding "membrane" work done by the prebuckling stress resultant $N_{\bar{x}}^{0i}$ in the $i$th segment during rolling deformations is:

$$W_m^i = \frac{1}{2}\int_{\bar{y}_i=0}^{b_i}\int_{\bar{x}=0}^{l} N_{\bar{x}}^{0i}(\omega_{\bar{z}}^2 + \omega_{\bar{y}}^2)\,d\bar{x}\,d\bar{y}_i \quad (83)$$

($i \neq$ web or other segments attached along $\bar{y} = \bar{z} = 0$).

The quantities $\omega_{\bar{z}}$ and $\omega_{\bar{y}}$ are the rotations about the $\bar{z}$ axis and $\bar{y}$ axis, respectively, and are given by:

$$\omega_{\bar{z}} = \frac{1}{2}\left(\frac{\partial v^*}{\partial \bar{x}} - \frac{\partial u^*}{\partial \bar{y}}\right)$$

$$\omega_{\bar{y}} = \frac{1}{2}\left(\frac{\partial u^*}{\partial \bar{z}} - \frac{\partial w^*}{\partial \bar{x}}\right). \quad (84)$$

*Bending and twisting energy.* In addition to the membrane energy-related modes just described, the

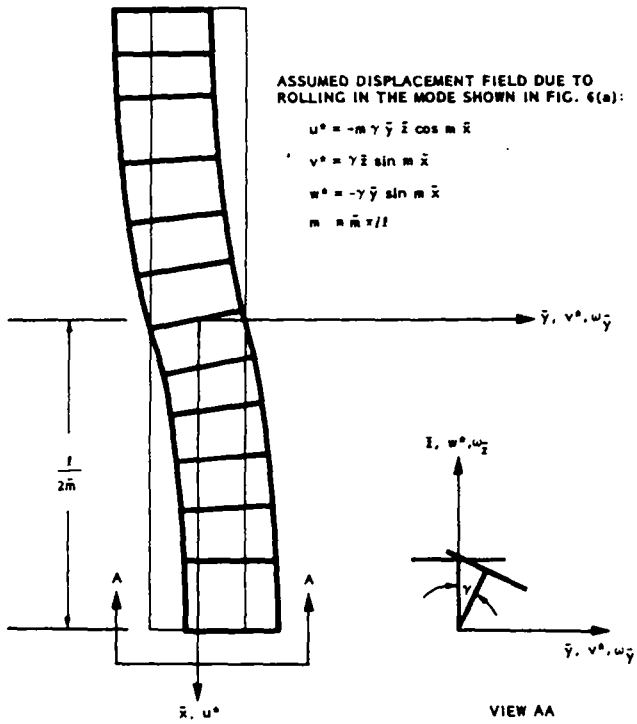


Fig. 12. In-plane bending of a flange induced by rolling of the stiffener in the mode shown in Fig. 6(a).

stiffener rolling deformations involve bending and twisting energy, that is, strain energy related to strains which vary through the thickness of each segment, and work done by the prebuckling stress resultant related to out-of-plane rotations of each stiffener segment. Only the bending and twisting energy of the stiffener web and other segments attached along the line $\bar{y} = \bar{z} = 0$ are included, since these components of energy are negligible compared to $U_m^i$ [eqn (81)] for the remainder of the stiffener cross-section. The bending and twisting strain energy of the web shown in Figs 11 and 12 is given by:

$$U_b^i = \frac{1}{2}\int_{\bar{y}_i=0}^{b_i}\int_{\bar{x}=0}^{l}[\kappa_{\bar{x}}, \kappa_{\bar{z}}, 2\kappa_{\bar{x}\bar{z}}][D^i]\begin{Bmatrix}\kappa_{\bar{x}}\\ \kappa_{\bar{z}}\\ 2\kappa_{\bar{x}\bar{z}}\end{Bmatrix} d\bar{x}\, d\bar{y}_i \tag{85}$$

($i$ = web or other segment attached along the line $\bar{y} = \bar{z} = 0$).

The coefficients of the $3 \times 3$ flexural rigidity matrix $D^i$ are called $C_{44}^i$, $C_{45}^i$, $C_{55}^i$, $C_{66}^i$ in eqn (68); they are given by eqns (70). Thus:

$$[D^i] \equiv \begin{bmatrix} D_{11}^i & D_{12}^i & 0 \\ D_{12}^i & D_{22}^i & 0 \\ 0 & 0 & D_{66}^i \end{bmatrix} \equiv \begin{bmatrix} C_{44}^i & C_{45}^i & 0 \\ C_{45}^i & C_{55}^i & 0 \\ 0 & 0 & C_{66}^i \end{bmatrix}. \tag{86}$$

These are the instantaneous flexural and twist rigidities of the $i$th stiffener segment, analogous to those for the panel skin referred to in the discussion associated with eqns (42)–(46). The expressions for changes in curvature and twist of the web are analogous to those for the panel skin:

$$\kappa_{\bar{x}} = -v^*_{,\bar{x}\bar{x}}; \quad \kappa_{\bar{z}} = -v^*_{,\bar{z}\bar{z}}; \quad \kappa_{\bar{x}\bar{z}} = -v^*_{,\bar{x}\bar{z}} \tag{87}$$

where $v^*$ is the displacement in the $\bar{y}$-direction, indicated in Figs 11 and 12. The work done by the prebuckling stress resultant during buckling of the web is:

$$W_b^i = \frac{1}{2}\int_{\bar{y}_i=0}^{b_i}\int_{x=0}^{l} N_{\bar{x}}^{0i} v_{,\bar{x}}^{*2}\, d\bar{x}\, d\bar{y}_i \tag{88}$$

($i$ = web or other segments attached along the line $\bar{y} = \bar{z} = 0$).

In PANDA rolling modes are assumed to occur only if the stiffener has a web which is perpendicular to the panel skin. The expressions (81) and (83) apply only to the portion of the stiffener attached to the end of this web. The cross-sections of these flange segments remain undeformed and initially plane sections of them remain plane during buckling deformations. However, note from Figs 11 and 12 that this plane rotates about the normal to the shell wall at the web attachment line. Therefore the entire cross-section of the stiffener (web and flange taken together) clearly warps. The expressions (85) and (88) apply only to the web. The bending and twisting energy of the rest of the stiffener cross-section is neglected compared to the membrane energy of the flange represented by eqn (81). This approximation seems valid as long as the segments are slender (width $\gg$ thickness).

*Introduction of displacement functions.* The various components of energy associated with the rolling mode shown in Figs 6, 11 and 12 are derived from eqns (81)–(88) with the assumed displacement field given in Fig. 12 and repeated here:

$$u^* = -m\gamma\bar{y}\bar{z}\cos m\bar{x} \tag{89a}$$

$$v^* = +\gamma\bar{z}\sin m\bar{x}$$

$$m = \bar{m}\pi/l \tag{89b}$$

$$w^* = -\gamma\bar{y}\sin m\bar{x}. \tag{89c}$$

If the height (width) of the web is called $b_w$ and one inserts the right-hand side of eqn (89a) (with $\bar{z} = b_w$) into eqn (81), one obtains for the membrane-type energy of each segment of the stiffener attached to the end of the web:

$$U_m^i = \frac{l}{4}(\gamma b_w)^2 m^4 \int_{\bar{y}_i=0}^{b_i} C_{11}^i \bar{y}^2\, d\bar{y}_i \quad (i \neq \text{web}). \tag{90}$$

$U_m^i$ can be evaluated once $\bar{y}$ as a function of $\bar{y}$ is known. For example, in the case of the T-shaped stiffener shown in Fig. 4(a), $\bar{y} = \bar{y}_2$ in Segment 2 and $\bar{y} = -\bar{y}_3$ in Segment 3. Therefore:

$$U_m^i = \frac{l}{4}(\gamma b_w)^2 m^4 C_{11}^i b_i^3/3 \quad (i = 2, 3). \tag{91}$$

If $C_{11}^{(2)} = C_{11}^{(3)}$, the total membrane energy $U_m = 2U_m^{(2)}$. This energy is simply the "EI" bending energy of a beam of depth equal to the width of the flange [$b_2 + b_3$ in Fig. 4(a)] deforming in its plane in a mode $(\gamma b_w)\sin m\bar{x}$. The bending and twisting energy of the web can be found, with use of eqns (85) and (87), to be:

$$U_b^i = \frac{l}{4}\left[C_{44}^w m^4 \gamma^2 \frac{b_w^3}{3} + 4C_{66}^w m^2 \gamma^2 b_w\right] \tag{92}$$

($w$ = "web"; $i$ = "web").

The corresponding "work done" terms, $W_m^i$ and $W_b^i$, are obtained from eqns (83), (84) and (88):

$$W_m^i = \frac{m^2 l}{4}(\gamma b_w)^2 \int_{\bar{y}=0}^{b_i} N_{\bar{x}}^{0i}\, d\bar{y}_i \quad (i \neq \text{web}) \tag{93}$$

$$W_b^i = \frac{m^2 l}{4}(\gamma b_w)^2 N_{\bar{x}}^{0i} b_w/3 \quad (i = \text{web}). \tag{94}$$

*Relation to panel skin deformation.* With no shear loading and the $A_{i6}$, $B_{i6}$, $D_{i6} = 0$ for $i \neq 6$ in eqn (37), the rotation $\gamma$, shown in Fig. 11, is related to the

amplitude $C$ of the sinusoidal deformation of the panel skin, $w_{skin} = 2C \sin ny \sin mx$ [eqns (50c) and (51) with $c = d = 0$], as follows:

$$\text{For stringers:} \quad \gamma = -2Cn$$

$$\text{For rings:} \quad \gamma = +2Cm \tag{95}$$

in which $n$ and $m$ are given by eqns (52). Through eqns (95), the components of rolling mode energy and work done by the prebuckling compression during buckling can be expressed in terms of the undetermined skin buckling amplitude $C$. The total potential energy $U - W$ has the same form as that given in eqn (54). The only difference is that the array element $a_{33}$, given for the panel skin in eqn (55f), has additional terms associated with stiffener deformations:

$$\begin{aligned} a_{33} &= [a_{33}]_{skin} \\ &+ \frac{2m^2n^2}{y_{max}}\left[m^2 b_w^2 \sum_{\substack{i=1 \\ i \neq \text{web}}}^{N^s}\left(\int_{\bar{y}=0}^{b_i} C_{11}^i[\bar{y}(\bar{y}_i)]^2 \, d\bar{y}_i\right)\right. \\ &+ C_{44}^w m^2 b_w^3/3 + 4C_{66}^w b_w \\ &\left. + b_w^2 \sum_{\substack{i=1 \\ i \neq \text{web}}}^{N^s}\left(\int_{\bar{y}=0}^{b_i} N_{\bar{x}pre}^{0i} \, d\bar{y}_i\right) + N_{\bar{x}pre}^{0w} b_w^3/3\right]_{stringer} \\ &+ \frac{2m^2n^2}{x_{max}}\left[n^2 b_w^2 \sum_{\substack{i=1 \\ i \neq \text{web}}}^{N^r}\left(\int_{\bar{y}=0}^{b_i} C_{11}^i[\bar{y}(\bar{y}_i)]^2 \, d\bar{y}_i\right)\right. \\ &+ C_{44}^w n^2 b_w^3/3 + 4C_{66}^w b_w \\ &\left. + b_w^2 \sum_{\substack{i=1 \\ i \neq \text{web}}}^{N^r}\left(\int_{\bar{y}=0}^{b_i} N_{\bar{x}pre}^{0i} \, d\bar{y}_i\right) + N_{\bar{x}pre}^{0w} b_w^3/3\right]_{ring} \end{aligned} \tag{96}$$

in which $\bar{y}(\bar{y}_i)$ indicates that $\bar{y}$ is a function of $\bar{y}_i$. In eqn (96), $x_{max}$ and $y_{max}$ have the meanings analogous to those in the discussion following eqn (49):

| Type of rolling instability | $x_{max}$ | $y_{max}$ |
|---|---|---|
| Local | $a_0$ | $b_0$ |
| Smeared stringers | $a_0$ | $b$ |
| Smeared rings | $a$ | $b_0$ |

The result in eqn (96) is obtained after division of both skin and stringer terms, derived from energy expressions, by the quantity $x_{max} y_{max}/4$.

The denominator on the right-hand-side of eqn (57) must also be modified by addition of the terms:

$$\begin{aligned} &-\frac{2m^2n^2}{y_{max}}\left[b_w^2 \sum_{\substack{i=1 \\ i \neq \text{web}}}^{N^s}\left(\int_{\bar{y}=0}^{b_i} N_{\bar{x}e}^{0i} \, d\bar{y}_i\right) + N_{\bar{x}e}^{0w} b_w^3/3\right]_{stringer} \\ &-\frac{2m^2n^2}{x_{max}}\left[b_w^2 \sum_{\substack{i=1 \\ i \neq \text{web}}}^{N^r}\left(\int_{\bar{y}=0}^{b_i} N_{\bar{x}e}^{0i} \, d\bar{y}_i\right) + N_{\bar{x}e}^{0w} b_w^3/3\right]_{ring} \end{aligned} \tag{97}$$

in which $N_{\bar{x}e}^{0i}$ and $N_{\bar{x}e}^{0w}$ are given by eqn (73). Expressions (95)–(97) apply only if $c = d = 0$. However, the eigenvalues including stiffener rolling are expected to be reasonably accurate for most practical cases involving combined in-plane loads which include shear.

*Rolling of stiffeners without participation of panel skin*

Figure 13 shows the coordinate system and positive displacement components $v$, $u^w$, $w^w$, $u^f$, $w^f$ in the web and flange. The following analysis is limited to stiffeners with T-shaped or L-shaped cross-sections. A special case of such a stiffener is a blade, which is a T- or L-shaped cross-section with a vanishingly small flange. The analysis is based on treatment of the web as a flexible annulus (a type of shell) and the flange as a very short cylindrical shell. Although Fig. 13 depicts the geometry for a ring, the analysis applies to stringers as well. In that case the radius of the short cylindrical shell that represents the flange is set equal to a very large number in PANDA.

*Assumptions.* The following assumptions are made with regard to the prebuckling and buckling modal strains and displacements:

(1) The prebuckling strains are assumed to be uniform over the web and uniform over the flange (although different prebuckling strain states exist in the web and flange).

(2) The buckling modal state is characterized by

*For the web:*

$$w_b^w(x, y) = [Cx^2 + Dx^2(1 - x/b_w)]\sin(\bar{n}\pi y/l) \tag{98}$$

$$e_x^b = 0 \tag{99}$$

$$e_{xy}^b = 0 \tag{100}$$

*For the flange:*

$$w_b^f(s, y) = u_b^w(x = b_w, y) + s\beta \sin(\bar{n}\pi y/l) \tag{101}$$

$$u_b^f(s, y) = \mp w_b^w(x = b_w, y) = u_b^f(y) \tag{102}$$

$$e_s^b = 0; \quad e_{sy}^b = 0 \tag{103}$$

in which $C$ and $D$ are coefficients to be determined by minimization of the total energy in the rolling stiffener. Quantities such as $x$, $y$, $s$ and $\beta$ and the various web and flange displacement components are indicated in Fig. 13 for both external and internal stiffeners. In terms preceeded with $\pm$ or $\mp$, the top sign corresponds to external stiffening and the bottom to internal stiffening. The quantity $u_b^w(x = b_w, y)$ signifies the value of $u^w$ evaluated at $x = b_w$ (see Fig. 13(b), for example).

*Strain energy.* The total strain energy of the stiffener is:

$$U = \frac{1}{2}\int_{y=0}^{l}\left(\sum_{i=1}^{N}\int_{\bar{y}_i=0}^{b_i}(\mathbf{e}_{pre} + \mathbf{e}^b)^T[C^i](\mathbf{e}_{pre} + \mathbf{e}^b)\, d\bar{y}_i\right) dy \tag{104}$$

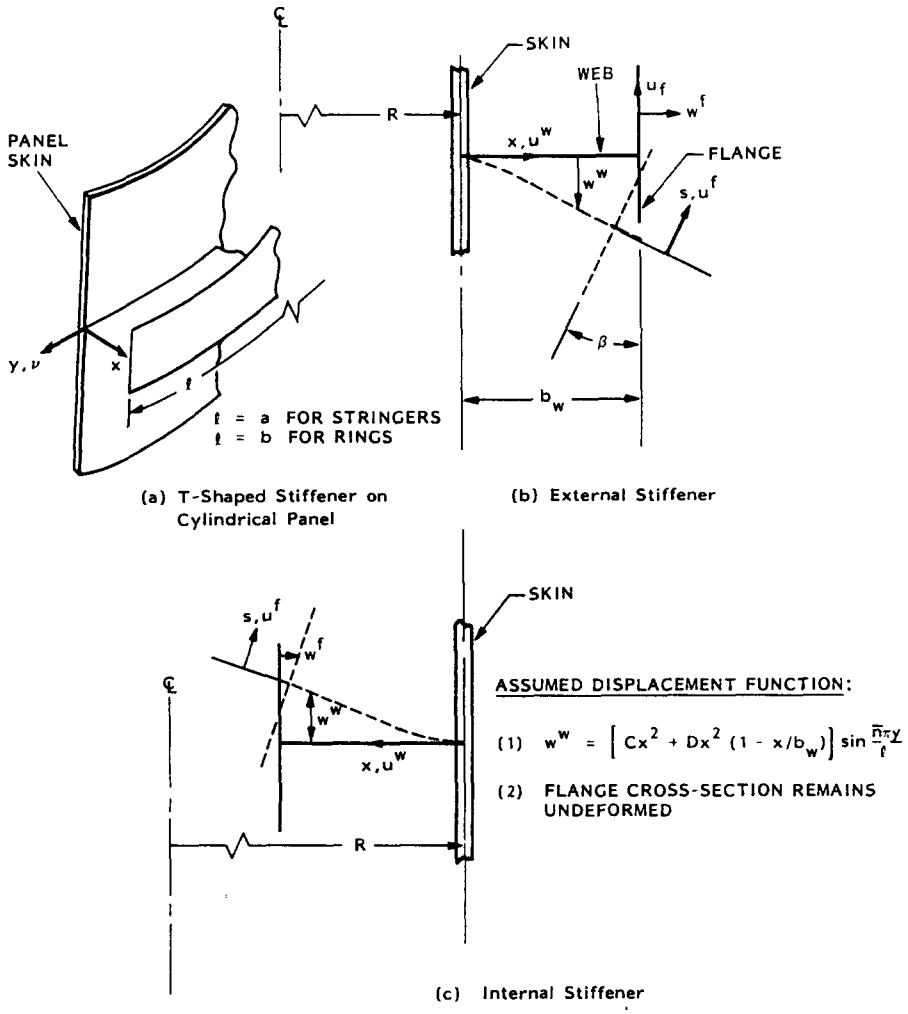


Fig. 13. Stiffener coordinates and displacement components for rolling analysis of the types shown in Figs 6(b) and (c) (no participation of the panel skin).

in which $N$ is the number of stiffener segments, $\bar{y}_i$ is the local stiffener segment coordinate shown in Fig. 4 ($\bar{y}_i = x$ in the web; $\bar{y}_i = s$ in the flange), and:

$$(\mathbf{e}_{pre})^T = \lfloor 0, e_y^0, 0, 0, 0, 0 \rfloor \tag{105}$$

$$(\mathbf{e}^b)^T = \lfloor 0, e_y^b, 0, \kappa_{\bar{y}}^b, \kappa_y^b, 2\kappa_{\bar{y}y}^b \rfloor . \tag{106}$$

Using eqns (104)–(106), one can write the strain energy of the $i$th segment of the stiffener in the simpler form:

$$U^i = \frac{1}{2}\int_{y=0}^{l}\int_{\bar{y}_i=0}^{b_i} [C_{22}^i(e_y^0 + e_y^b)^2 + C_{44}^i(\kappa_{\bar{y}}^b)^2 + 2C_{45}^i\kappa_{\bar{y}}^b\kappa_y^b + C_{55}^i(\kappa_y^b)^2 + C_{66}^i(2\kappa_{\bar{y}y}^b)^2]\,d\bar{y}\,dy. \tag{107}$$

Note that because the web and flange are here being treated as shell components, $C_{22}^i$ and $C_{55}^i$ are identified with the long dimension, $l$, of the stiffener while $C_{44}^i$ is identified with the width, $b_i$. This is the opposite nomenclature from that used in the previous section.

*Strain–displacement relations for buckling analysis.* The strain–displacement relations to be used here are of the Novoshilov–Sanders type. They are the same as those used in BOSOR4 [13] and BOSOR5 [14].

*For the web:*

$$e_x = u' + (w'^2 + \gamma^2)/2 = 0 \tag{108a}$$

$$e_y = \dot{v} \pm u/r + (\psi^2 + \gamma^2)/2 \tag{108b}$$

$$e_{xy} = \dot{u} + r(v/r)' + w'\dot{w} = 0 \tag{108c}$$

$$\kappa_x = w'' \tag{108d}$$

$$\kappa_y = \dot{\psi} \pm w'/r \tag{108e}$$

$$2\kappa_{xy} = 2(-w'' \pm \dot{w}/r) \tag{108f}$$

$$\psi = \dot{w} \tag{108g}$$

$$\gamma = (\dot{u} - v' \mp v/r) \tag{108h}$$

in which $(\,)' \equiv \mathrm{d}(\,)/\mathrm{d}x$ and $(\dot{}) \equiv \mathrm{d}(\,)/\mathrm{d}y$.

*For the flange:*

$$e_x = 0 \tag{109a}$$

$$e_y = \dot{v} + w/R_f + (\psi^2 + \gamma^2)/2 \tag{109b}$$

$$e_{xy} = \dot{u} + r(v/r)' + w'(\dot{w} - v/R_f) = 0 \tag{109c}$$

$$\kappa_x = w'' \tag{109d}$$

$$\kappa_y = \ddot{w} - \dot{v}/R_f \tag{109e}$$

$$2\kappa_{xy} = 2(-w'' + v'/R_f) \tag{109f}$$

$$\psi = \dot{w} \tag{109g}$$

$$\gamma = (\dot{u} - v')/2 \tag{109h}$$

in which $(\,)' \equiv \mathrm{d}(\,)/\mathrm{d}x$ and $(\dot{}) \equiv \mathrm{d}(\,)/\mathrm{d}y$ and in which superscript $b$ has been dropped for convenience.

*Analysis of the web.* The assumptions that $e_x = e_{xy} = 0$ [eqns (99), (100)] along with eqns (108a) and (108c) can be used to determine $u^w$ and $v^w$, given $w^w$ [eqn (98)]. After some algebraic manipulations one obtains:

$$u^w = [-2(C+D)^2x^3/3 + 3(C+D)Dx^4/(2b_w) - 9(D/b_w)^2x^5/10]\sin^2(\bar{n}\pi y/l) \tag{110}$$

$$v^w = -(\bar{n}\pi/l)[(C+D)^2x^4/6 - 2(C+D)Dx^5/(5b_w) + (D/b_w)^2x^6/5]\sin(\bar{n}\pi y/l)\cos(\bar{n}\pi y/l). \tag{111}$$

With use of eqns (107), (108), (110) and (111), one obtains for the strain energy of the web (including the effect of the prebuckling stress resultant in the $y$-direction, $N^{0w}$):

$$U^{\text{web}} = \frac{l}{4}\{C^2[p_1 + p_2 + 4C^w_{44}b_w + q_i + q_2 + 4q_3 - s_1 + s_2] + CD[p_1/5 + p_2/3 - 4C^w_{44}b_w + q_1/3 - q_3 + s_1 - s_2] + D^2[p_1/10 + p_2/21 + 4C^w_{44}b_w + q_1/21 + 2q_3/5 + s_1/5 + s_2/4]\} \tag{112}$$

in which:

$$p_1 = \mp N^{0w}b_w^4/(3r_{\text{ave}})$$
$$p_2 = n^2N^{0w}b_w^5/5 \tag{113a}$$

$$q_1 = b_w^5(C^w_{55}n^4 + 4C^w_{66}n^2/r^2_{\text{ave}})/5$$
$$s_1 = 4C_{45}n^2b_w^3/3 \tag{113b}$$

$$q_2 = \mp b_w^4n^2(C^w_{55} + 4C^w_{66})/r_{\text{ave}}$$
$$s_2 = \pm 4\,C_{45}b_w^2/r_{\text{ave}} \tag{113c}$$

$$q_3 = b_w^3(C^w_{55}/r^2_{\text{ave}} + 4C^w_{66}n^2)/3 \tag{113d}$$

where $r_{\text{ave}}$ is the average radius of the web,

$$r_{\text{ave}} = (R + R_f)/2 \tag{114}$$

and $n$ is given by:

$$n = \bar{n}\pi/l. \tag{115}$$

In eqn (113a, b) the stress resultant in the web $N^{0w}$ is comprised of two parts, a fixed part and a part to be multiplied by the eigenvalue,

$$N^{0w} = N^{0w}_{PRE} + \lambda N^{0w}_{e}. \tag{116}$$

*Analysis of the flange.* From the assumption that $e_{xy} = 0$ [eqn (103)] along with eqns (109c) and (102), an expression for $v$ can be derived. From eqn (102), it is known that:

$$u^f = \mp Cb_w^2\sin(\bar{n}\pi y/l). \tag{117}$$

Integration of eqn (109c) yields:

$$v^f = \pm(n\pi/l)Cb_w^2s\cos(\bar{n}\pi y/l) + v^w(x = b_w) \tag{118}$$

in which $v^w(x = b_w)$ signifies the value of $v^w$ evaluated at $x = b_w$ (see Fig. 13). The last term on the right-hand-side of eqn (118) drops out when integration over $y$ is performed.

With use of eqns (107), (109), (117) and (118), one obtains for the strain energy of the flange (including the effect of the prebuckling stress resultant in the $y$-direction $N^{0f}$):

$$U^f = \frac{l}{4}\{C^2[f_1c_2 + f_2c_3 + f_3c_4^2 + c_5(2+e)^2] + CD[-f_1c_6 - f_3(2e)c_4 - 2(2+e)c_5 + c_7] + D^2[f_1c_1 + f_3e^2 + c_5 - 4c_7]\} \tag{119}$$

in which:

$$f_1 = \sum_{\substack{i=1\\ i\neq\text{web}}}^{N} N_i^{0f}b_i^3/3, \quad f_2 = \sum_{\substack{i=1\\ i\neq\text{web}}}^{N} N_i^{0f}b_i$$

$$f_3 = \sum_{\substack{i=1\\ i\neq\text{web}}}^{N} C^i_{22}b_i^3/3, \quad f_4 = \sum_{\substack{i=1\\ i\neq\text{web}}}^{N} C^i_{55}b_i^3/3$$

$$f_5 = \sum_{\substack{i=1\\ i\neq\text{web}}}^{N} C^i_{66}b_i \tag{120}$$

and:

$$c_1 = n^2b_w^2$$
$$c_2 = c_1(2+e)^2$$
$$c_3 = c_1b_w^2 \mp 4b_w^3/(3\,R_f)$$
$$c_4 = c_1 + 2e$$
$$c_5 = c_1(n^2f_4 + 4f_5)$$
$$c_6 = c_1 2(2+e)$$
$$c_7 = \pm f_2b_w^3/(3R_f) \tag{121}$$

with:

$$e = \mp b_w / R_f \tag{122}$$

where $R_f$ is the radius of the very short cylindrical shell that represents the flange.

As in the case of the web, the prebuckling stress resultant in the flange is comprised of two parts, a fixed part and a part to be multiplied by the eigenvalue.

$$N_i^{0f} = N_{iPRE}^{0f} + \lambda N_{ie}^{0f}. \tag{123}$$

*Lowest eigenvalue.* The lowest eigenvalue $\lambda$ for stiffener rolling instability without participation of the skin can be obtained by insertion of the right-hand-side of eqn (116) into eqn (112), insertion of the right-hand-side of eqn (123) into eqn (119), minimization of the sum of $U^{web}$ and $U^f$ with respect to the coefficients $C$ and $D$, and determination of the lowest root of the quadratic equation in $\lambda$ that represents the vanishing of the determinant of the coefficient matrix of the two simultaneous homogeneous equations in $C$ and $D$.

*Axisymmetric rolling instability.* Axisymmetric rolling instability of rings can be calculated by the setting of $n$ in eqns (113) and (121) equal to zero. It is interesting to note that rolling instability is possible in the case of internally pressurized cylindrical shells with external rings even though the stresses everywhere in the shell, web and flange are tensile.

*Acknowledgements*—Part of the effort to develop PANDA was sponsored by the U.S. Air Force, Aeronautical Systems Division, Wright Patterson AFB, Ohio, under Contract AFFDL F33615-76-C-3105. Dr Narenda S. Khot (AFWAL/FIBRA) was project engineer. Much of the support for the development of PANDA came from the 1980–1982 Lockhead Independent Development Programs. For this support the author is greatly indebted to Bill Sable.

## REFERENCES

1. D. Bushnell, PANDA—interactive program for minimum weight design of stiffened cylindrical panels and shells. *Comput. Struct.* **16**, 167–185 (1983).
2. D. Bushnell, PANDA2 program for minimum weight design of stiffened, composite, locally buckled panels. *Comput. Struct.* **25**, 469–605 (1987).
3. L. H. Donnell, A new theory for the buckling of a thin cylinder under axial compression and bending. *Trans. Am. Soc. mech. Engrs* **56**, 795–806 (1934).
4. R. M. Jones and J. C. F. Hennemann, Effect of prebuckling deformations on buckling of laminated composite circular cylindrical shells. *AIAA Jnl* **18**, 110–115 (1980); see also *Proc. AIAA/ASME 19th SDM Conf.*, pp. 370–379 (1978).
5. B. O. Almroth, Influence of edge conditions on the stability of axially compressed cylindrical shells. *AIAA Jnl* **4**, 134–140 (1966).
6. J. W. Hutchinson, Plastic buckling. In *Advances in Applied Mechanics*, Vol. 14 (Edited by C. S. Yih), pp. 69–144. Academic Press, New York (1974).
7. R. M. Jones, *Mechanics of Composite Materials*. McGraw-Hill, New York (1975).
8. M. Baruch and J. Singer, Effect of eccentricity of stiffeners on the general instability of stiffened cylindrical shells under hydrostatic pressure. *J. mech. Engng Sci.* **5**, 23–27 (1963).
9. D. O. Brush and B. O. Almroth, *Buckling of Bars, Plates and Shells*. McGraw-Hill, New York (1975).
10. A. B. Burns, Optimum stiffened cylinders for combined axial compression and internal or external pressure. *J. Spacecraft Rockets* **5**, 690–699 (1968).
11. M. Pappas and A. Allentuch, Pressure hull optimization using general instability equation admitting more than one longitudinal buckling half-wave. *J. Ship Res.* **19**, 18–22 (1975).
12. M. Booton and R. C. Tennyson, Buckling of imperfect anisotropic circular cylinders under combined loading. *AIAA Jnl* **17**, 278–287 (1979).
13. D. Bushnell, Stress, stability, and vibration of complex, branched shells of revolution. *Comput. Struct.* **4**, 399–435 (1974).
14. D. Bushnell, BOSOR5—program for buckling of elastic-plastic complex shells of revolution including large deflections and creep. *Comput. Struct.* **6**, 221–239 (1976).